Coupled Eulerian Wall Film-Discrete Phase model for predicting respiratory droplet generation during a coughing event

Nguyen Dang Khoa
Interdisciplinary Graduate School of Engineering Sciences, Kyushu University

Kuga, Kazuki
Faculty of Engineering Sciences, Kyushu University

Inthavong, Kiao
School of Engineering, Mechanical and Automotive, RMIT University

Ito, Kazuhide
Faculty of Engineering Sciences, Kyushu University

https://hdl.handle.net/2324/7174458

KYUSHU UNIVERSITY

1 **Coupled Eulerian Wall Film-Discrete Phase model for predicting the**

2 **respiratory droplets generation during the coughing event**

3

4 Nguyen Dang Khoa[a)*], Kazuki Kuga (久我一喜)[b)], Kiao Inthavong[c)], Kazuhide Ito (伊藤一

5 秀)[b)]

6

7 [a)] Interdisciplinary Graduate School of Engineering Sciences, Kyushu University, Fukuoka,

8 Japan

9 [b)] Faculty of Engineering Sciences, Kyushu University, Fukuoka, Japan

10 [c)] School of Engineering, Mechanical and Automotive, RMIT University, Melbourne, Australia

11

12 * Corresponding authors

13 E-mail: ndkhoa@kyudai.jp (NDK)

14 IGSES, Kyushu University, 6-1, Kasuga-koen, Kasuga, Fukuoka, 816-8580, Japan

15

16

Abstract

Infectious respiratory diseases have long been a serious public health issue, with airborne transmission via close person-to-person contact being the main infection route. Coughing episodes are an eruptive source of virus-laden droplets that increase the infection risk of susceptible individuals. In this study, the droplet generation process during a coughing event was reproduced using the Eulerian wall film (EWF) model, and the absorption/expulsion of droplets was tracked using the discrete phase model (DPM). A realistic numerical model that included the oral cavity with teeth features and the respiratory system from the throat to the first bifurcation was developed. A coughing flow profile simulated the flow patterns of a single coughing episode. The EWF and DPM models were coupled to predict the droplet formation, generation, absorption, and exhalation processes. The results showed that the large droplet number concentration was generated at the beginning of the coughing event, with the peak concentration coinciding with the peak cough rate. Analysis of the droplet site of origin showed that large amounts of droplets were generated in the oral cavity and teeth surface, followed by the caudal region of the respiratory system. The size of the expelled droplets was 0.25–24 μm, with the peak concentration at 4–8 μm. This study significantly contributes to the realm on the site of origin and localized number concentration of droplets after a coughing episode. It can facilitate studies on infection risk assessment, droplet dispersion, and droplet generation mechanisms from other sneezing or phonation activities.

36

39

40

I. INTRODUCTION

Infectious respiratory diseases have long been a significant public health concern. This includes instances of plagues, measles, tuberculosis, influenza, severe acute respiratory syndrome coronavirus (SARS-CoV), Middle East respiratory syndrome coronavirus (MERS-CoV), and the most recent SARS-CoV-2 (Churchyard et al., 2017; Piret & Boivin, 2021). Person-to-person airborne transmission of respiratory viruses can occur via direct or indirect contact, respiratory droplets, and droplet nuclei transmission (Dhand & Li, 2020; C. C. Wang et al., 2021). Infected patients can expel pathogen carriers into the ambient environment via respiratory activities such as breathing, talking, phonating, singing, sneezing, or coughing (Wei & Li, 2016; Stadnytskyi et al., 2021). Once in the surrounding environment, viral-laden droplets can remain airborne for an extended period and transported by indoor airflow to the effective breathing zone of residents, and subsequently inhaled at various exposure levels, as reported by previous studies that were comprehensively reviewed by Inthavong (Inthavong, 2020). During the expiratory phase, the infection risks are associated with the (1) droplet number concentration, (2) size distribution, (3) content of infectious agents, and (4) performance frequency (Morawska, 2006). Besides, more recent studies underscore the dependence of disease transmission on infective dose threshold of the virus (SeyedAlinaghi et al., 2022) and the viral shedding rate (Widders et al., 2020). Thus, quantitative studies are required to determine the pathogen susceptibility targeting each activity.

4

60   The threat of coughing-related infections has gained public attention, being extensively

61   studied over the past decades owing to its possibility for the eruptive release of many pathogens

62   in a short period (Stadnytskyi et al., 2021). When coughing, the sequent build-up of expiratory

63   flow velocity, reaching a Reynolds number of 10^4 (Bourouiba et al., 2014), expulses

64   compressed air through the open mouth. Due to the high speed, droplets are produced in the

65   oral cavity due to shear-induced surface-wave instabilities (Wei & Li, 2016; Pöhlker et al.,

66   2021). The stripped droplet parcels follow the air stream and escape to the environment through

67   the open mouth or are re-absorbed into the mucus layer. Virus-laden droplets are generally

68   deposited in the respiratory tract after inhalation (H. Li et al., 2022; C. C. Wang et al., 2021).

69   The mucus clearance process (i.e., coughing) can trigger the re-emittance of deposited virions

70   or the local transmission of progeny viruses shed by infected cells (Schaefer & Lai, 2022).

71   Therefore, the number concentration and size distribution of droplets from coughing have

72   gained significant attention from the scientific community. A review of studies over the past 20

73   years has indicated significant scatter (Yang et al., 2007; Chao et al., 2009; Morawska et al.,

74   2009; Johnson et al., 2011; Lindsley et al., 2012; Zayas et al., 2012), which can be attributed

75   to the heterogeneity of measurement techniques, sampling methods, or intersubject variability.

76   More recently, facilitated by advanced techniques, the realm of measuring ejected cloud

77   characteristics and generated droplet properties from oral activities in an indoor environment

78   has been embarked upon to deliver a comprehensive understanding during the pandemic epoch

5

79　(Wang et al., 2020; Archer et al., 2022; Harrison et al., 2023; Bahramian & Ahmadi, 2023).

80　Drawing upon the properties of generated droplets from experimental studies, computer-aided

81　approaches have been expanded to explore further the deleterious effects of these droplets in

82　the context of disease transmission. Among them, Computational Fluid Dynamics (CFD) has

83　been universally adopted for the numerical investigation of the contagion risk of coughing.

84　Most studies have investigated the cough-jet stream characteristics and fate of expiratory

85　droplets in an enclosed environment (H. Li et al., 2021; Payri et al., 2021; Nie et al., 2022;

86　Aljabair et al., 2023; Nishandar et al., 2023), or the distance-based exposure risks between

87　residents (Calmet et al., 2021; Mariam et al., 2021; Hossain et al., 2023; X. Li et al., 2023). As

88　can be seen, up to date, both experimental and numerical endeavors have extensively advanced

89　our understanding of droplet size distribution and their behavior under varying microclimatic

90　conditions within an enclosed environment. Nonetheless, the site origin and generation

91　mechanism of these droplets in the respiratory tract have yet to be discussed in the listed studies.

92　　Against this background, further numerical studies have been conducted on the interactions

93　between high-speed, chaotic exhaled air and the liquid-layer lining the inner surface of the

94　airway (i.e., the mucus layer) during the coughing episode. The two most common methods

95　adopted are the volume of fluid (Paz et al., 2019; Rajendran & Banerjee, 2019; Pairetti et al.,

96　2021; Yi et al., 2021) and Eulerian wall film (EWF) models (Paz, Suárez, Parga, et al., 2017;

97　Paz, Suárez, & Vence, 2017; Ren et al., 2018, 2020, 2022; Anzai et al., 2022). These studies

98   provide an understanding of the respiratory droplet generation process, the effects of mucus

99   properties on cough clearance efficiency, and the impact of airway deformation. To facilitate

100   the assessment of the infection risks of virus-laden droplets, it is crucial to qualitatively and

101   quantitatively investigate the origin of respiratory droplets during expiratory events (i.e.,

102   coughing). Furthermore, the realistic and comprehensive characteristics of the target

103   respiratory airway model should be considered to ensure the accuracy of the cough-jet stream

104   and expelled droplet features.

105   In this study, the EWF model and Lagrangian discrete phase model (DPM) were coupled

106   to characterize the following: (1) fluid flow profiles of coughing; (2) number concentration,

107   size distribution, and locality of generated and expelled droplet particles during coughing; and

108   (3) absorption efficiency of stripped droplets. The results establish a link between the high viral

109   load of the infected respiratory tract and the possibility of such viral pathogens being released

110   into the environment by coughing. Subsequently, the infection risk can be determined for

111   different respiratory viruses.

112   **II. MATERIALS AND METHODS**

113   **A. Numerical model geometry**

114   The realistic airway model comprised a computed tomography (CT)-based trachea-

115   bronchus model and oral cavity produced by the open-source DAZ Studio software (DAZ

116   Productions, Inc.) shown in Fig. 1. During coughing, various oral shapes and sizes were

117   observed (Dbouk & Drikakis, 2020). In this study, the newly developed oral cavity model

118   mimicked the configuration of a slightly open mouth with dimensions of L = 4.7 cm and H =

119   0.85 cm (Fig. 1) to similarly match the data provided by experimental measurements from high-

120   speed imaging (Dbouk & Drikakis, 2020). The total area of the open mouth of 3.76 cm^2 was

121   within the range of 4 ± 0.95 cm^{2,} as stated in a previous study (Seminara et al., 2020). In

122   addition, the teeth attributes were integrated to provide the most realistic traits of the oral cavity

123   (Fig. 1). The realistic trachea-bronchus model was created from CT scans, and details on the

124   process are available in the previous study by Ito (Ito, 2016). This trachea-bronchus model, in

125   combination with the nasal cavity, has been validated by our research group, providing reliable

126   results in diverse research themes (C. Wang et al., 2020; Yoo & Ito, 2022; Kuga et al., 2021,

127   2022, 2023; Murga et al., 2023; Khoa, Li, et al., 2023).

128   **B. Grid design information**

129   The discretization process was executed using the poly-hex core elements, which proposed

130   the CFD simulation with higher accuracy at a reduced computational cost (Zore et al., 2019).

131   The accuracy in the vicinity of the wall was enhanced by applying ten prism layers. This hybrid

132   mesh has been successfully used to predict airflow and particle transportation/deposition

133   simulation of the respiratory tract (Khoa, Phuong, et al., 2023; Khoa, Li, et al., 2023).

134   According to the mesh independence test, the mesh size of 15.5 million cells was selected for

135   subsequent simulation in this study, more detailed information can be found in Fig. S1

8

136   (Supplementary Material). This analysis strikes the balance between the computational burden

137   and prediction accuracy.

C. Numerical simulation of airflow pattern

139   The unsteady, incompressible, and isothermal fluid flow in the human respiratory tract was

140   obtained by solving the Reynolds-averaged Navier–Stokes equations.

$$\frac{\partial \overline{U_i}}{\partial x_i} = 0 \tag{1}$$

$$\frac{\partial \overline{U_i}}{\partial t} + \frac{\partial \overline{U_i U_j}}{\partial x_j} = -\frac{1}{\rho_g}\frac{\partial \overline{p_g}}{\partial x_i} + \frac{\partial}{\partial x_j}\left[\left(\nu + \nu_T\right)\left(\frac{\partial \overline{U_i}}{\partial x_j} + \frac{\partial \overline{U_j}}{\partial x_i}\right)\right] \tag{2}$$

141   where $\overline{U}$ is the mean velocity; u' is the fluctuating components; and p_g, ρ_g, ν, and ν_T are

142   the pressure, density, kinematic viscosity of the fluid, and turbulent viscosity, respectively.

143   This study selected the turbulent model of the shear stress transport (SST) k-ω. This model

144   has been used to predict adverse pressure gradient flow, strong curvature, and swirling flow in

145   airway systems, as shown in previous experiments (Phuong & Ito, 2015; Elcner et al., 2016).

146   The coughing flow profile was obtained from field measurements of Gupta for male subjects,

147   as shown in Fig. 2A (Gupta et al., 2009). From the empirical equation, the coughing flow rate

148   was allocated to four inlets according to the flow weighting of each lobe of the lung proposed

149   in (Shelley et al., 2014), and reasonably applied in our study (Khoa, Li, et al., 2023), as shown

150   in Fig. 2B. This procedure was implemented via a user-defined function (UDF) macro in

151   ANSYS Fluent. The numerical boundary conditions for the coughing airflow simulation are

9

152   listed in Table I.

153   **D. Eulerian Wall Film simulation**

154   In a coughing episode, an excessive fluid flow velocity is rapidly produced and subjected

155   to turbulence and high shear stress at the interface between the airstream and thin liquid film

156   (mucus/saliva). Under such conditions, Kelvin–Helmholtz instabilities occur, which cause

157   waves with an escalating amplitude on the surface of a thin liquid film (Pöhlker et al., 2021).

158   Droplets form from the crest of these waves in a multimodal mode and are carried by the flow.

159   The droplet generation mechanism can be predicted using the EWF model, in which thin

160   liquid mucus layers were hypothesized to be aligned on the inner surface of the oral-tracheal

161   model. The governing equation of the EWF model is as follows (ANSYS, Inc. 2022):

$$\frac{\partial \rho_l h}{\partial t} + \nabla_s . \left(\rho_l h \vec{V}_l \right) = \dot{m}_s \tag{3}$$

$$\frac{\partial \rho_l h \vec{V}_l}{\partial t} + \nabla_s . \left(\rho_l h \vec{V}_l \vec{V}_l + \overline{D}_V \right) = -h \nabla_s P_L + \rho_l h \vec{g}_\tau + \frac{3}{2} \vec{\tau}_{fs} - \frac{3\mu_l}{h} \vec{V}_l + \vec{q}_s \tag{4}$$

$$\overline{D}_V = \frac{\partial}{\partial s} \int_0^h v_l^2 dy \tag{5}$$

$$P_L = P_{gas} + P_h + P_\sigma \tag{6}$$

$$P_h = -\rho h \left(\vec{n}.\vec{g} \right) \tag{7}$$

$$P_\sigma = -\sigma \nabla_s . \left(\nabla_s h \right) \tag{8}$$

162   where ρ_l is the film density, h is the film height, V_l is the mean film velocity, and m_s is the

163   mass source per unit wall area owing to droplet collection, film separation, film stripping, and

164   phase change. In Equation 4, D_V is the differential advection term computed based on the

165   quadratic film velocity with fluctuating velocity $v_l(s,y,t)$, in which s is the horizontal flow

166   direction and y is the vertical direction (Kakimpa et al., 2015). The term P_L is the mucus film

167   pressure, g_τ is the gravity component, τ_{fs} is the shear force at the film–liquid interface, μ_l is the

168   viscosity, q_s is the momentum source, σ is the surface tension, P_σ is the pressure exerted by the

169   surface tension, P_h is the gravity component normal to the wall, and n is the normal vector.

170   The reliability of applying the EWF model in anticipating the interaction between the

171   coughing stream jet and lining fluid is emphasized through supplementary simulations

172   conducted using a simplified airway model. The simulation results were subsequently

173   compared with experimental data, and additional information on this validation process is

174   elaborated upon in Fig. S2 (Supplementary Material).

175   In the context of our primary simulation, the EWF model was included with the fluid flow

176   at the beginning of the coughing episode. The simulation was applied to the total inner surface

177   of the numerical domain, including the teeth surface. In general, the mucus thickness varies

178   along the airway system. However, to simplify the simulation, a constant thickness of 30 μm

179   was used to represent the mucus layer in the throat, larynx, trachea, and bifurcation, based on

180   previous studies (Paz, Suárez, Parga, et al., 2017; Paz, Suárez, & Vence, 2017; Ren et al., 2022;

181   Anzai et al., 2022). For the oral cavity, the saliva thickness ranged from 11.3 to 68.9 μm, as

182   proposed by the research of Assy (Assy et al., 2022). For the teeth surface, the saliva thickness

183   was assigned based on early experimental data (Collins & Dawes, 1987), which ranged from

184   2.59 to 4.44 μm following the mandibular, maxillary, left, or right position of teeth. The saliva

185   and mucus layers were assumed to be water with a density of 998.2 kg/m^3 and viscosity of

186   0.001 kg/m s.

187   Shear-induced droplet generation was considered through the high velocity and turbulent

188   flow, causing the instability of the lining mucus/saliva layers and leading to droplets peeling

189   from the crests of the formed waves. This process was defined by the initial parameters given

190   in Table II. Among them, the critical shear stress is the main factor that governs the number

191   concentration of generated droplets. A parametric analysis was required prior to the main

192   simulation to determine an appropriate value for the simulation, which is delivered in Fig. S3

193   (Supplementary Material). Notably, this analysis was significantly influenced by the individual

194   morphological characteristics considered in this study. Then, a value of 5 Pa was specified for

195   the critical shear stress, which imposed the limit that any region subjected to shear stress greater

196   than 5 Pa would trigger the shedding of mucus/saliva layers into droplets. In addition, a

197   diameter coefficient, which specifies the droplet size range (ANSYS, Inc. 2022), was also

198   determined by experiencing the parametric analysis with a value of 0.0003 (Fig. S4,

199   Supplementary Material). Finally, the film time-step size was automatically assigned by

200   ANSYS Fluent using adaptive time-stepping functions, which controlled the time-step size to

201   be small enough to ensure that the maximum Courant number during the simulation was less

202   than 1. The continuous generation of mucus/saliva layers beneath the epithelial cells was

203   neglected, which indicated no refill of mucus/saliva layers after being dispossessed.

204   **E. Discrete Phase model simulation**

205   The EWF model was coupled with the DPM to track the trajectories of droplets stripped

206   from the liquid film. Forces acting on the body were used to predict the droplet transportation,

207   absorption, and exhalation characteristics of the oral-tracheal model. The Lagrangian discrete

208   phase of the particle trajectories was computed by Equation 9.

$$\frac{d\vec{u}_p}{dt} = \vec{F}_D + \vec{F}_G + \vec{F}_s \tag{9}$$

209   where the subscript p is the droplet phase and $\vec{F}_D$ is the drag force per unit particle mass

210   derived from Stokes' drag law, expressed in Equation 10.

$$\vec{F}_D = \frac{18\mu}{\rho_p d_a^2} \frac{C_D \, \mathrm{Re}_p}{24} \left(\vec{U} - \vec{u}_p \right) \tag{10}$$

211   where μ is the air viscosity, $\vec{U}$ is the fluid flow velocity, $\vec{u}_p$ is the droplet velocity, d_a is

212   the aerodynamic droplet diameter, ρ_p is the droplet density, C_D is the drag coefficient, and Re_p

213   is the particle Reynolds number.

214   The second term, $\vec{F}_G$, denotes the gravitational settling. The third term, $\vec{F}_s$, is Saffman's

215   lift force due to shear on a unit mass basis. The lift force was adapted from a previous study by

216   Li and Ahmadi (A. Li & Ahmadi, 1992), and is a generalization of the expression provided by

217   Saffman (Saffman, 1965), expressed as Equation 11.

13

$$\vec{F}_S = \frac{5.188v^{1/2}\rho d_{ij}}{\rho_p d_a \left(d_{lk}d_{kl}\right)^{1/4}}\left(\vec{U}-\vec{u}_p\right) \tag{11}$$

218   where d_{ij}, d_{lk}, and d_{kl} are deformation rate tensors.

219   The aerodynamic diameter and number of tracked droplets were determined based on the

220   EWF simulation. The droplets were defined with a unit density (1000 kg/m^3), equal to that of

221   pure water. The fate of the droplets was considered as exhaled via the mouth opening or was

222   re-absorbed into the mucus layer; hence, the "escape" boundary condition was assigned to the

223   mouth opening, and the "perfect trap" condition was applied as the wall boundary conditions.

224   The evaporation and breakup of the droplets were negligible. The droplets were continuously

225   generated during the simulation; therefore, the velocity, size, and spatial and temporal

226   information of the droplets stripped from the mucus layer were recorded using the UDF macro

227   for each time-step.

228   The generated, exhaled, and absorbed percentages, denoted as $\eta_{G\text{-}i}$, $\eta_{E\text{-}i}$, and $\eta_{A\text{-}i}$, can be

229   expressed by Equations 12, 13, and 14, respectively.

$$\eta_{G-i} = \frac{N_{G-i}}{N_G}\times 100\% \tag{12}$$

$$\eta_{E-i} = \frac{N_{E-i}}{N_E}\times 100\% \tag{13}$$

$$\eta_{A-i} = \frac{N_{A-i}}{N_A}\times 100\% \tag{14}$$

230   where $N_{G\text{-}i}$, $N_{A\text{-}i}$, and $N_{E\text{-}i}$ are the number of droplets generated, absorbed, and exhaled that

231   belong to region i, which corresponds to the regions defined in Fig. 1. N_G, N_A, and N_E are the

232   total stripped, absorbed, and exhaled droplets after a single coughing episode (duration of 0.5

14

233   s), respectively. The size distribution of the coughed droplets was multimodal; accordingly, the

234   droplet size bin was identified to establish the size distribution percentage of the generated,

235   exhaled, and absorbed droplets (η_{G-s}, η_{E-s}, and η_{A-s}), given in Equations 15, 16, and 17,

236   respectively.

$$\eta_{G-s} = \frac{N_{G-s}}{N_G} \times 100\% \tag{15}$$

$$\eta_{E-s} = \frac{N_{E-s}}{N_E} \times 100\% \tag{16}$$

$$\eta_{A-s} = \frac{N_{A-s}}{N_A} \times 100\% \tag{17}$$

237   where N_{G-s}, N_{A-s}, and N_{E-s} are the number of droplets generated, absorbed, and exhaled,

238   respectively, which decreases in the size bin, as listed in Table III.

239   The size distribution of exhaled droplets can be calculated by dividing the number of

240   droplets within the specific size bin by the logarithm of the droplet size class interval (dN_{E-}

241    $_s/dLogD$). Finally, the exhaled droplet size distribution was normalized with the total cough

242   exhaled volume (1,000 cm^3) to obtain the number concentration divided by the logarithm of

243   the droplet size class interval ($dC_{NE-s}/dLogD$).

244   **III. RESULTS**

245   **A. Coughing fluid flow characteristics**

246   The results of the coughing fluid flow features are depicted in Fig. 3 at the start of the

247   coughing episode at 0.01 s, cough peak flow rate (CPFR) at 0.077 s, and near the end of the

248   coughing event at 0.4 s. Notably, the velocity magnitude and distribution herein are described

249   at the instantaneous times. At the onset of coughing (Fig. 3A), the culminated velocity occurred

250   at the bifurcation, trachea, glottis, and throat regions with a value of 3 m/s. At CPFR, the spatial

251   distribution of the jet stream remained, but the magnitude increased by almost 13-fold up to 40

252   m/s. In the final coughing stage, the coughing velocity rapidly decreased to less than 3 m/s in

253   identical acceleration regions.

254   In the oral cavity (Fig. 3B), the airstream accelerated in the throat region and impacted the

255   palate and bends following the curvilinear shape of the oral ceiling. The expulsive flow that

256   escaped the oral region was primarily distributed at the bottom of the mouth opening. Reserve

257   flow also formed in the basal region near the mouth opening, which contributed to the swirling

258   flow at the mouth opening (Fig. 3B). Due to the flow features toward the ceiling of the oral

259   cavity, the maxillary teeth are expected to endure the high-velocity flow during the cough. Fig.

260   3C shows the two-dimensional flow distribution for the maxillary teeth, which revealed that

261   the high-velocity fluid flow attacked the inner surface of the molars, premolars, canines, and

262   incisors.

263   **B. Droplet generation mechanism during coughing**

264   The rapid increase in the flow rate due to coughing induces substantial shear stress on the

265   airway wall, closely linked to the droplet production criteria in the EWF model simulation. The

266   relationship between shear stress, mucus thickness, and stripped droplets is presented in Fig. 4,

267   which describes the instantaneous value of each variable. At 0.01 s (Fig. 4A), the low coughing

268 velocity resulted in a modest shear stress of less than 5 Pa on the airway wall, which failed to

269 meet the minimum threshold to produce droplets; hence, the droplets were not observed and

270 the mucus/saliva thickness remained in its original state. At CPFR (Fig. 4B), the cough ejection

271 velocity increased to 40 m/s, which induced significant shear stress on the wall surfaces.

272 Multiple airway surfaces experienced shear stress levels greater than 5 Pa, which fulfilled the

273 criterion for droplet generation off the thin liquid film on the oral-airway surfaces. Accordingly,

274 the mucus/saliva thickness decreased to almost 0 μm and droplets simultaneously emerged in

275 the corresponding regions (Fig. 4B). The complex and uneven surface of the oral-airway model

276 produced an uneven distribution of the peak shear stresses. This completely removed the

277 mucus/saliva layers in several specific regions while the remaining areas preserved their initial

278 liquid film thickness. Droplet production decreased significantly at 0.15 s (Fig. 5C) due to the

279 mucus/saliva layers dissipating, following the former intense erosion process during CPFR.

280 **C. Properties of generated droplets during coughing**

281 The relationship between the coughing flow profile and droplet production was correlated

282 to understand the droplet generation process better. The instantaneous number of droplets

283 stripped from the mucus/saliva layers due to the coughing flow rate during the single coughing

284 episode (~0.5 s) is shown in Fig. 5A. The results demonstrate that the coughing flow rate

285 rapidly increased in the early stage of coughing. In contrast, droplet generation lagged and

286 didn't start until 0.04 s with an initial rapid rise. The number of droplets produced increased

17

287 rapidly in parallel with the coughing flow rate and formed a sharp slope, with the peak almost

288 coinciding with the CPFR (at approximately 0.077 s). After reaching their peaks, the cough

289 flow rate and number of stripped droplets exhibited a downward trend. The number of droplets

290 produced rapidly dropped to almost 0 at 0.25 s, in contrast to the cough flow that gradually

291 decreased to 0 taking 0.5 s. After the single coughing episode, 11,594,566 droplets were

292 generated (Table IV). The instantaneous position of the droplets during different times during

293 the cough are shown in Fig. 5B for time, t = 0.025, 0.04, 0.077, and 0.2 s, where the droplets

294 are colored by diameter. The results indicate an early appearance of droplets in the bifurcation

295 and throat regions (at 0.025 s). At 0.04 s, a dense population of droplets was observed in the

296 bifurcation and oral cavity, which corresponds to the airway curvature of the palate region in

297 line with the flow distribution in the oral cavity. At CPFR at t = 0.077 s, the oral-airway model

298 is filled with a very high density of droplets due to the rapid droplet production (shown in Fig.

299 5A). At t = 0.2 s, most of the droplets were re-absorbed into the mucus/saliva layers or

300 transported by the coughing flow toward the oral region and released into the external

301 environment via the mouth opening. Hence, fewer droplets are found in the airway compared

302 to the oral cavity. Furthermore, the droplet size was less than 10 μm for the entire coughing

303 episode.

304   One advantage of this study is that it provides details on the origin of the stripped droplet

305 during the coughing event, illustrated in Fig. 5C. The oral region was identified as the primary

306   source of droplets (up to 46.8%) during the cough. In the remaining regions, the droplet

307   production levels were similar (approximately 11.9–14.3%), slightly reducing towards the

308   bifurcation region. The large amount of stripped droplets in the oral cavity is attributed to

309   higher shear stresses (exceeding 5 Pa) than in other regions. Fig. 5D shows the total surface

310   area (cm^2) of each region subjected to shear stress of >5 Pa, where the oral cavity exhibited the

311   highest surface area. Therefore, more droplets were produced from the saliva film in the oral

312   airway region.

313   The percentage of droplets generated per droplet diameter size bin can be estimated using

314   Equation 15, as shown in Table IV. Most droplets produced were in the size interval of 4–8 μm

315   (approximately 78.01%), followed by 2–4 and 8–16 μm, respectively. The droplets in the size

316   bin of <1 μm had a low percentage of 0.078–0.181%, while for the larger size bins (>16 μm),

317   the rate was only 0.169%.

318   **D. Properties of exhaled droplets during coughing**

319   An analysis of the expelled droplet concentration for different droplet diameters was

320   performed and compared with experimental measurements of Yang (Yang et al., 2007). In the

321   experimental work, 54 volunteers of varying ages and genders coughed into a sampling bag

322   with a well-controlled relative humidity; thus, the coughed droplets retained their original size.

323   Fig. 6A shows the number concentration of droplets at the mouth opening plotted against the

324   average droplet size and compared with Yang (Yang et al., 2007). The EWF model closely

Physics of Fluids

AIP Publishing

325   matched the profile with the measured exhaled number concentration. There was a sharp

326   increase in the number concentration for droplet sizes approximately at 2 μm before reaching

327   a peak concentration (approximately 2,500/cm^3) at 4–8 μm. After the peak, a downward trend

328   was observed, and the cutoff diameter where no droplets were expelled was >10 μm.

329   The source of droplets expelled to the environment is shown in Fig. 6B, where the oral

330   cavity (including the teeth surface) was responsible for the largest amount of droplets exhaled

331   into the environment (up to 75%). The amount gradually reduced for the geometry moving

332   posteriorly toward the caudal airway; specifically, 12.3% originated from the throat, followed

333   by the larynx (approximately 8.3%), trachea, and bifurcation (approximately 2.2%),

334   respectively.

335   Most exhaled droplets, 73.1%, were between 4-8 μm due to the highest percentage of

336   droplets produced in this range (Table IV). For smaller droplets, the exhalation rates were

337   12.8% and 8.9% for size bins of 2–4 μm and 8–16 μm, respectively. Despite the low production

338   rate of droplets in the size bin of <1 μm, the appearance of these small droplets in the exhaled

339   breath was 0.49–0.79%.

340   The spatial distribution of the droplets that escaped through the mouth during the coughing

341   is illustrated in Fig. 6C, where the different droplet colors denote the source location. The

342   results show that the oral cavity is the primary location of the expelled droplets, and the droplets

343   exit through the entire space of the mouth opening. For the other airway regions (throat, larynx,

20

344 trachea, and bifurcation), the expelled droplets mainly dispersed through the lower half of the

345 mouth opening. There was a small scattering of droplets in the upper half of the mouth opening.

346 Despite the significant variation in the vertical distribution of droplets expelled, the horizontal

347 distribution in the lower half was consistent. This distribution was due to the oral cavity shape

348 and the exhaled jet stream found in the lower half of the mouth opening (shown in Fig. 3).

349 **E. Absorbed efficiency of droplets during coughing**

350 The total number of droplets absorbed onto the mucus/saliva layers was 10,128,559 (Table

351 IV), accounting for approximately 87.3% of the total droplets produced by the cough. The

352 primary absorption region was the oral cavity (including the teeth surface), with 47.8%. In

353 contrast, in the remaining regions, the absorption efficiency significantly decreased by

354 approximately four-fold in the 11.2–14.1% range. Most of the generated droplets re-absorbed

355 into the oral region's saliva layer can be associated with the complex morphology of this region,

356 which prevented the smooth movement of the droplets.

357 Fig. 7B shows the droplet absorption efficiency categorized by the region where the

358 droplets originated from (e.g. slice color indicates the droplet source location). In general,

359 droplets were immediately re-absorbed back into its own region where they were generated.

360 For example, 87.5% of droplets produced in the oral cavity re-absorbed in its region, and that

361 of the throat, larynx, trachea, and bifurcation, the re-absorption rate was 88.2%, 91.9%, 93.1%,

362 and 100%, respectively.

363   The cough-jet stream began from the tracheal bifurcation, and the oral region had the

364   greatest exposure to all droplets originating from lower regions, including the throat (5.3%),

365   larynx (4.2%), trachea (1.8%), and bifurcation (1.3%). This geometry and flow feature explains

366   the lack of absorbed droplets from geometrically lower regions (e.g. upstream flow) than the

367   region itself since the jet flow transports the droplets from the bifurcation to the oral cavity.

368   Droplets with sizes of 4–8 μm (Table IV) were the most re-absorbed due to the greater number

369   of generated droplets in this size bin. For the other size bins, the absorption rate was similar to

370   its generation rate.

371   Fig. 8 shows the deposition pattern on specific airway regions based on where the droplets

372   were produced. Deposition in the oral cavity showed that the focal absorption region occurred

373   in the palate regardless of the droplet origin. Most droplets in the throat tended to accumulate

374   in the upper and branching regions. In the larynx and trachea, there was a high rate of re-

375   absorption from itself. Only the droplets produced by itself were re-absorbed for the bifurcation,

376   and most were observed in the left bifurcation.

377   Generally, the cough-jet stream influenced droplet deposition in the oral airway, and the

378   droplet absorption patterns coincided with the high-velocity regions, as discussed in the

379   previous section.

380   **F. Role of teeth surface in the simulation of droplet generation during coughing**

381   The results reveal the critical role of the oral cavity in droplet generation, emission, and

382 absorption. This raises the question of the contribution of the teeth surface to the areas of

383 interest in this study. In this section, the droplet generation, absorption and exhalation from the

384 oral cavity were divided into the teeth surface and the remaining portion of the oral airway

385 surface (shown in Fig. 9A). The total of 46.8% of droplets that were produced from the oral

386 cavity (from Fig. 5C), were found to originate evenly between the teeth surface and remaining

387 portion (approximately 23%).

388 The instantaneous shear stress at 0.04 s and 0.077 s is given in Fig. 10A. Shear stress >5

389 Pa was observed on the maxillary incisor surface in the early stage of the coughing event (0.04

390 s). A high shear rate was found on the inner surface of the maxillary teeth, including the incisors,

391 canines, and molars, at the CPFR (0.077 s). Consequently, many droplets were stripped from

392 the saliva layers along the inner side of the maxillary teeth surface (Fig. 10B). This

393 phenomenon is closely associated with the cough-jet stream, which impacted the upper jaw, as

394 discussed in the previous section.

395 For the expelled droplets (Fig. 9B), approximately 40% was derived from the teeth's surface.

396 This was attributed to the droplets that formed on the teeth surface, especially on the incisors,

397 which travelled a short distance without any obstacles to the mouth opening. For the re-

398 absorption capacity, the larger surface area of the remaining portion of the oral region caused

399 a larger number of droplets to re-absorb (approximately 27%). In comparison, 21% of droplets

400 re-absorbed onto the teeth surface.

401 Figure 11 presents both the quantitative analysis and spatial distribution of droplets

402 absorbed on the teeth surface. Primarily, the quantitative analysis serves to delineate the

403 proportion of total absorbed droplets on the teeth surface, which was generated from distinct

404 regions within the model. The findings revealed that out of the total number of droplets

405 absorbed on the teeth surface, 81.02% of absorbed droplets originated from this area.

406 Subsequently, droplets emanating from the oral cavity constituted 14.79% of the total absorbed

407 droplets on the teeth surface. The percentage gradually reduced for the posterior regions and

408 reached 0.45% for the bifurcation, which implies a limited quantity of droplets stemmed from

409 this region absorbed onto the teeth surface. In addition, the spatial distribution of the droplet

410 deposition on the teeth surface indicates that most droplets tended to settle on the inner surface

411 of the maxillary teeth or partially in the mandibular molars and canines, regardless of their

412 origin.

413 **IV. DISCUSSIONS**

414 The coupled EWF-DPM model was applied to explore droplet generation and flow

415 behavior during a single coughing event, where the origin and local number concentration of

416 the generated, absorbed, and expelled droplets were determined. This study first analysed the

417 coughing flow rate, which provides insight into the droplet generation process during coughing.

418 The rapid development of airflow velocity along the airway and oral cavity subjected the

419 surface walls to high shear stress, which caused the stripping of mucus/saliva layers into

420   droplets. The airstream accelerated through the narrow airway lumen (e.g., trachea, glottis, and

421   throat regions), consistent with a previous study (Kou et al., 2018). Thus, the predicted fluid

422   flow is recognized as a constant feature of coughing in terms of the velocity distribution but

423   would vary in magnitude depending on the lumen diameter of individual airway structures. In

424   the oral cavity, this study included the teeth geometry, which has been lacking in reported

425   simulation studies of the fluid flow characteristics during coughing. Our results indicate a

426   strong interaction between the cough-jet stream and maxillary teeth surface, which could

427   influence droplet generation and absorption/exhalation.

428   The shear-induced droplet generation due to the high-speed velocity is one of the four

429   generation mechanisms that mainly occurs in the main bronchus, trachea, and larynx regions

430   (Pöhlker et al., 2021). The results revealed an essential connection between the shear stress and

431   the number concentration of generated droplets, summarized as follows. The higher the

432   coughing flow rate, the greater the shear stress, and the larger the number of droplets generated.

433   This relationship indicates the uncertainty of the generated droplet number concentration owing

434   to the coughing flow profile, particularly at the CPFR. For instance, the significant diversity

435   between individuals and genders has been recorded for coughing parameters, such as the peak

436   velocity, peak velocity time, and coughing duration by field measurements (Han et al., 2021).

437   These variations are expected to affect droplet generation. In addition, the fidelity of the

438   numerical domain needs to be considered. Earlier simulation studies used an idealized model

439   that proposed a smooth shear stress distribution on the wall surface (Anzai et al., 2022). The

440   study by Ren et al. (Ren et al., 2022) reported a nonuniform distribution of shear stress on a

441   realistic lower airway wall. The results showed heterogeneities in spatial distribution and

442   magnitude of shear stress compared with ours; consequently, the droplet generation differed.

443   Nevertheless, the coughing flow profile, realistic attributes, and intersubject variability

444   presented challenges, and the simulation results need to be benchmarked against the

445   experimental results.

446   For infection risk assessment, it is crucial to understand the origins of droplets during

447   expiratory activities within a specific area and to quantify the droplets generated from each

448   source (Morawska, 2006). For coughing, droplet-released sources are well established and

449   consist of the lungs, trachea, nasopharynx-larynx, and nasal and oral passages (Stadnytskyi et

450   al., 2021; Zhou & Zou, 2021). However, the exact location of droplet generation/exhalation

451   and their localized number concentration remain uncertain. Our droplet generation analysis

452   indicates that the most likely sources of droplets produced during coughing were the oral cavity

453   and teeth surface. Although common respiratory viruses primarily occur in the epithelial cells

454   of the respiratory system (Alexander-Brett & Holtzman, 2015), evidence suggests high viral

455   loads of SARS-CoV-2 in saliva samples from an asymptomatic cohort and the active replication

456   of infected cells in the oral cavity (Huang et al., 2021). In addition, previous clinical studies

457   have detected SARS-CoV-2 in patient saliva (To et al., 2020; Wölfel et al., 2020; Wyllie et al.,

458   2020). Thus, from our results, the high infection risk of SARS-CoV-2 may be associated with

459   a high droplet concentration in the oral cavity. Apart from the oral cavity, the deposition site

460   can be determined in the airway system of the potential host (C. C. Wang et al., 2021), but this

461   depends on the aerosols or virus-laden droplet size. Droplets from the deposition regions may

462   cause the re-emission of progeny viruses shed by infected cells (Schaefer & Lai, 2022).

463   Therefore, the possibility of transmission droplets originating from the respiratory system was

464   indicated by our analytical data, where considerable quantities of exhaled droplets were

465   recorded from the throat, larynx, trachea, and bifurcation. The results showed that the

466   generation sites of droplets tended to be in a particular position rather than evenly distributed.

467   The site of origin affected the potential direction of the droplet cloud during a cough. Our

468   results showed that exhaled droplets from the oral cavity escaped to the surroundings at all

469   locations and angles from the mouth opening; hence, the droplets travelled further and

470   dispersed widely. Meanwhile, exhaled droplets stripped from the respiratory airway exhibited

471   a downward direction as they exited the mouth into the ambient environment. This

472   phenomenon is expected to direct the droplets to the ground outside. Thus, our location-specific

473   results can inform studies on the threat of coughing-related infections in indoor environments.

474   In addition to identifying the origin site, the local number concentration and size

475   distribution of droplets exhaled during coughing were determined. Based on the literature

476   review, these two parameters were estimated for a varied population and measurement

27

477 techniques. As summarized in Fig. S5 (Supplemental Material), the field measurement data

478 were scattered broadly regarding the size distribution and number concentration. In particular,

479 the peak number concentration was recorded in the 4–8 μm range proposed by Yang and Chao

480 (Yang et al., 2007; Chao et al., 2009). This peak shifted to 0.75–2 μm in the experiment by

481 Morawska and Johnson (Morawska et al., 2009; Johnson et al., 2011). The highest number

482 concentration was recorded at a much smaller size, at 0.3 μm measured by Lindsley and Zayas

483 (Lindsley et al., 2012; Zayas et al., 2012). In addition, the number concentration among the

484 references indicated significant variations. Therefore, our analysis was validated by recruiting

485 one specific experimental data from Yang et al (2007). Both experimental and simulated data

486 showed that a 4–8 μm droplet size was formed and exhaled at a high number concentration

487 during coughing. Within this size range, the expelled droplets would travel further into the

488 environment and suspend for longer, enhancing the exposure risk of residents in a confined

489 space (Jones & Brosseau, 2015; Dhand & Li, 2020; Bourouiba, 2021). Nevertheless, the

490 lifetime and size of droplets have a complex relationship with many environmental factors,

491 including temperature, humidity, and ventilation mechanisms (Jayaweera et al., 2020;

492 Bahramian, 2023). Once inhaled by a susceptible person, fine aerosols (<5 μm) have a high

493 possibility of escaping the defence mechanism of the upper airway and penetrating the lower

494 airway, which is often associated with higher severity, morbidity, and fatality (Zuo et al., 2020;

495 Sosnowski, 2021). A more significant amount of viral genomes of common respiratory viruses

28

496 have been revealed in fine aerosols (<5 μm) compared with larger ones (Gralton et al., 2013;

497 Yan et al., 2018). Information regarding the site origin and local number concentration was

498 revealed by our analysis, which may not be possible in field measurements with volunteers

499 owing to ethical and technical barriers.

500   Our simulation data showed that one issue that should be addressed in droplet generation,

501 absorption, and exhalation studies is the inclusion of detailed oral cavity and teeth features.

502 The oral cavity was a significant source of droplet expulsion; however, due to its complex

503 anatomy with the existence of the teeth, the region provided a source for droplet absorption,

504 thereby contributing to the mitigation of droplet emissions from caudal respiratory areas. By

505 eliminating realistic features or simplifying the oral cavity, the high local concentrated

506 absorption regions may shift to the larynx-throat region, according to our data and a previous

507 simulation (Guo et al., 2020), allowing more droplets to be expelled. Thus, the realistic

508 anatomy of the oral cavity alters the number concentration and spread angle of ejected droplets,

509 thereby changing the dispersion and migration characteristics of the expelled droplets.

510   Throughout the discussion points, it is noteworthy that the data was obtained upon the

511 assumption of one single cough event. Concerns may arise regarding whether introducing a

512 successive coughing process would impact the results. In this context, the previous

513 experimental research revealed the second cough characteristics with a homogeneous profile

514 but weakened mechanical effectiveness, such as cough peak flow rate and expired volume

Physics of Fluids

515 (Gupta et al., 2009; Hegland et al., 2013). This weakening was prolonged until the end of the

516 cough epoch. Upon these conditions, outcome variation can be anticipated as following points:

517   (i)   Within the coughing flow patterns, continuous accelerations are expected to occur

518   during each coughing episode, with the highest magnitude in the first cough and a

519   precipitous decline in the subsequent cough events.

520   (ii) Regarding the generated droplet number concentration, although a number

521   concentration increase is conceivable, it would not anticipated to yield a significant

522   deviation from the current results. This expectation is rooted in the observation that

523   the mucous membrane almost diminished after the initial coughing event, as indicated

524   in Fig.4. Additionally, the WSS exerted on the respiratory wall may fall below the

525   given CSS and be insufficient to trigger the droplet stripping.

526   (iii) In terms of droplet behaviors (absorbed or expelled), consecutive acceleration of fluid

527   flow can result in the variation of the absorption rate due to the inertia, subsequently

528   leading to the corresponding alternations in the escaped rate.

529   Henceforth, subjecting the current research to successive cough simulations while

530 maintaining consistent initial conditions is expected to yield modest variations. Hence, it may

531 be reasoned that the applicability of the results may be regarded as akin to the current findings

532 under the assumption of a single cough process.

533 **V. CONCLUSIONS**

534   Detailed information on the droplet generation, exhalation, and absorption behavior in a

535   realistic oral-tracheal model was elucidated using the coupled EWF-DPM model. The main

536   points of the analysis are summarised as follows:

537   • The EWF model reliably predicted the interaction between the free stream and

538   liquid film lining by validating it against measured data. Coupled with the DPM

539   model, the concentration profile of exhaled droplets from the mouth opening after

540   a coughing episode could represent experimental data.

541   • The morphometry fidelity of the oral-tracheal model and the coughing flow rate

542   affects the cough-jet stream and is expected to alter droplet generation,

543   transportation/absorption, and exhalation.

544   • Shear stress at the liquid film-air interface is a critical factor governing the droplet

545   generation properties. Therefore, appropriate values as the input criteria for the

546   EWF and benchmarking against experimental data are required.

547   • The oral and teeth surface were primary locations for droplet generation. While

548   other regions of the respiratory system showed a much lower droplet production

549   rate. The rates gradually decreased toward the posterior regions.

550   • Most exhaled droplets were 4–8 μm in diameter. Droplet sizes of <1 μm and >10

551   μm were also detected but were much fewer upon exhalation through the mouth

552   opening.

31

553   • Including the teeth surface provided a more realistic simulation, directly influencing

554   the droplet number concentration that could be expelled through the mouth opening.

555   Our simulation can be a foundation for further studies on droplet cloud generation and the

556   transmission of viral genomes in the environment from sneezing, speaking, singing, or

557   phonation activities. It also provides quantitative and qualitative assessments of infection risk

558   based on the site of origin, size distribution, and localised number concentration.

559   **VI. FIGURES**
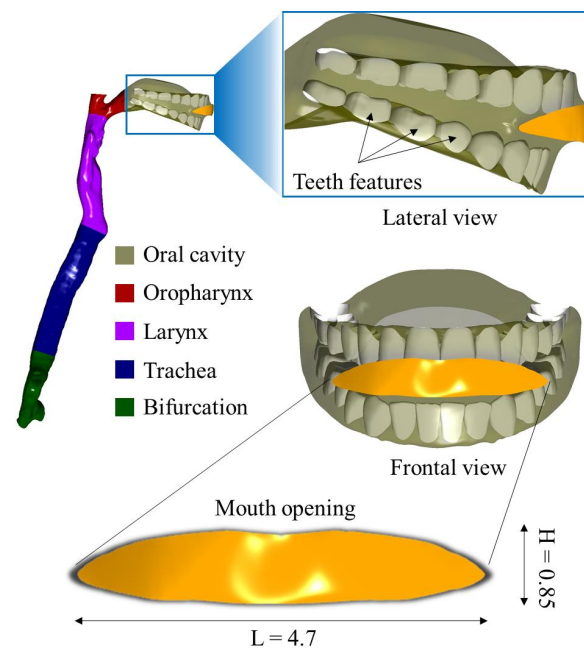
FIG. 1. Outline of the simulation model

560

561

562
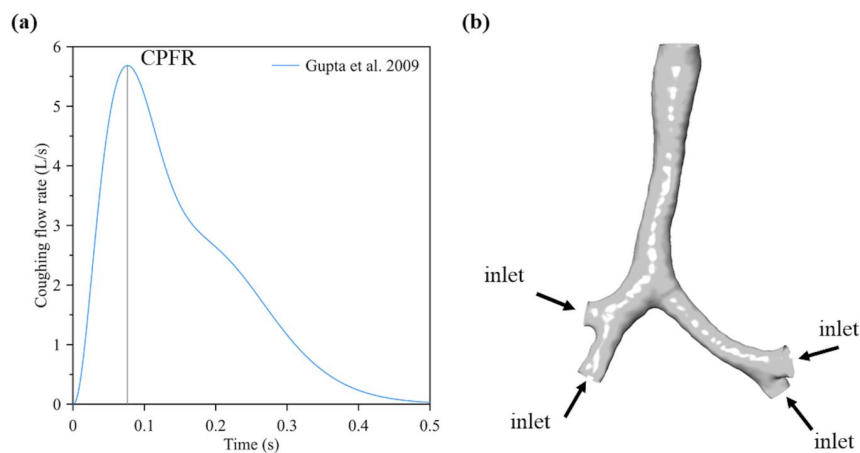
FIG. 2. (a) Coughing flow rate following the previous field measurement. (b) The description of inlet boundary conditions.

563

564

565

566

567

568

569

570

571

572

573

33
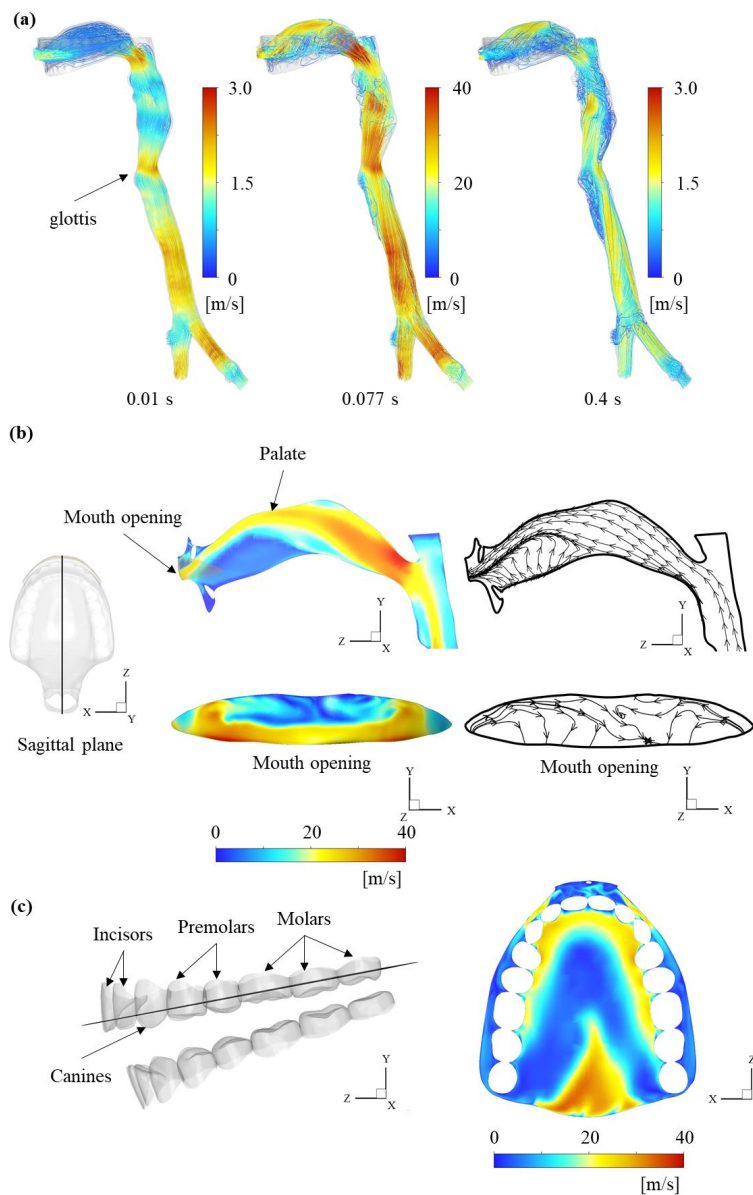
FIG. 3. (a) Instantaneous streamline velocity distribution at the specific time during coughing. (b) Instantaneous 2D flow features in the oral cavity and the mouth opening, and (c) in the vicinity of the maxillary teeth surface at the CPFR (0.077 s)

574

Wall Shear Stress (WSS) Mucus/saliva thickness Droplet source

(a)

0.01 s

(b)

0.077 s

(c)

0.15 s

0.0   5.0   0.0   69

[Pa]   [μm]
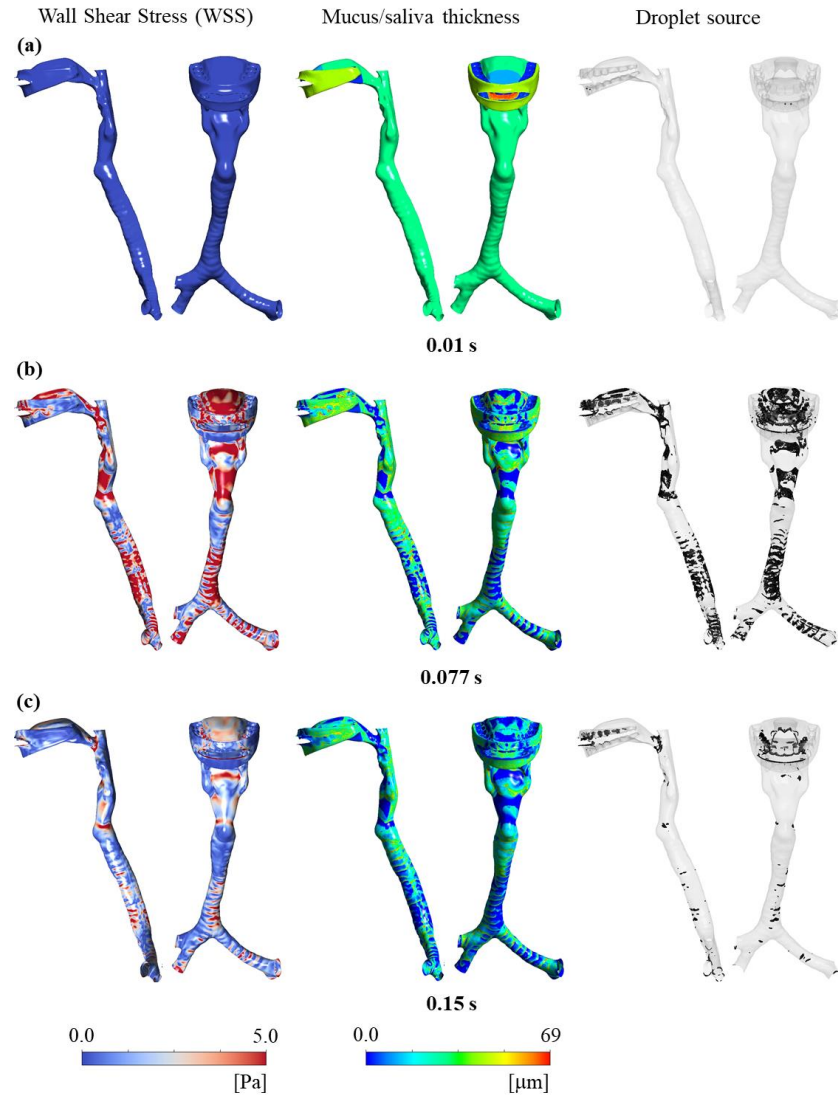
FIG. 4. The immediate distribution of wall shear stress (left), mucus/saliva thickness (middle), and initial position of stripped droplets (right) at (a) 0.01 s, (b) 0.077 s, and (c) 0.15 s.

575

35

Physics of Fluids
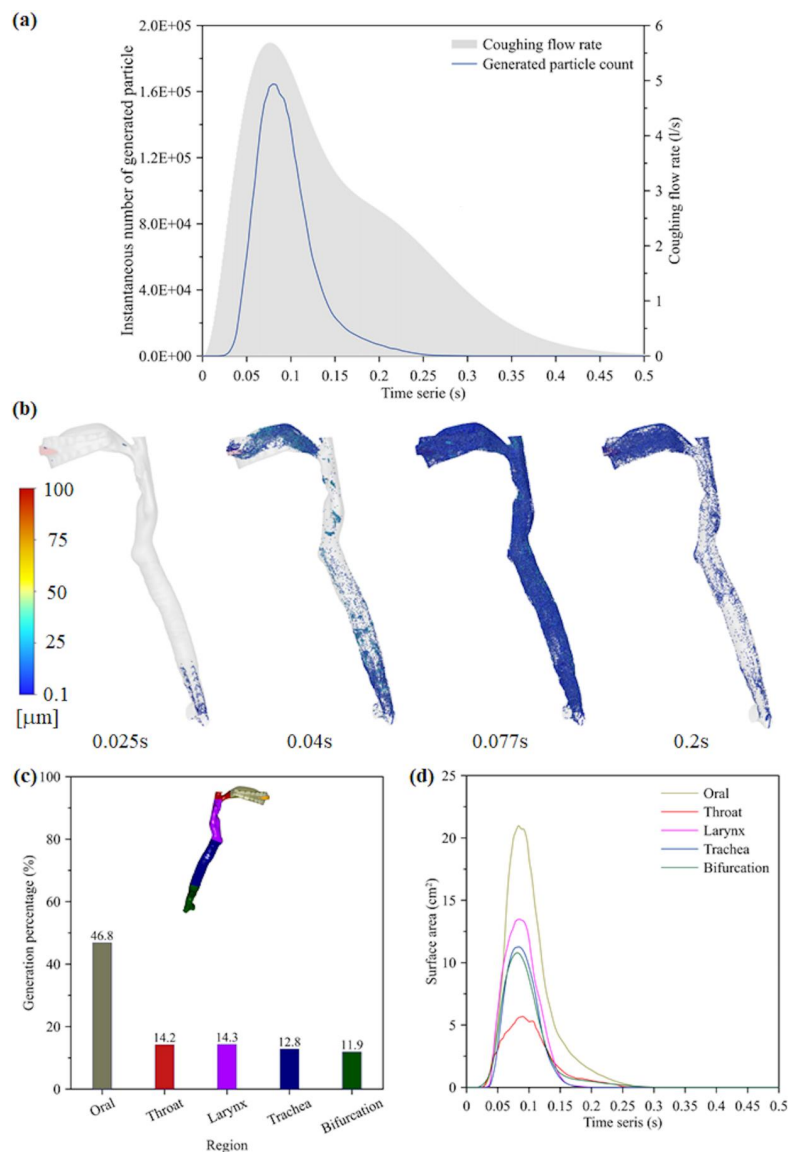
FIG. 5. (a) The instantaneous number of generated droplets during the cough event associated with the coughing flow rate. (b) Instantaneous positions of droplets at different times during the cough. (c) The percentage of droplets produced from their origin. (d) The surface area of each airway region that experienced wall shear stresses greater than 5 Pa.
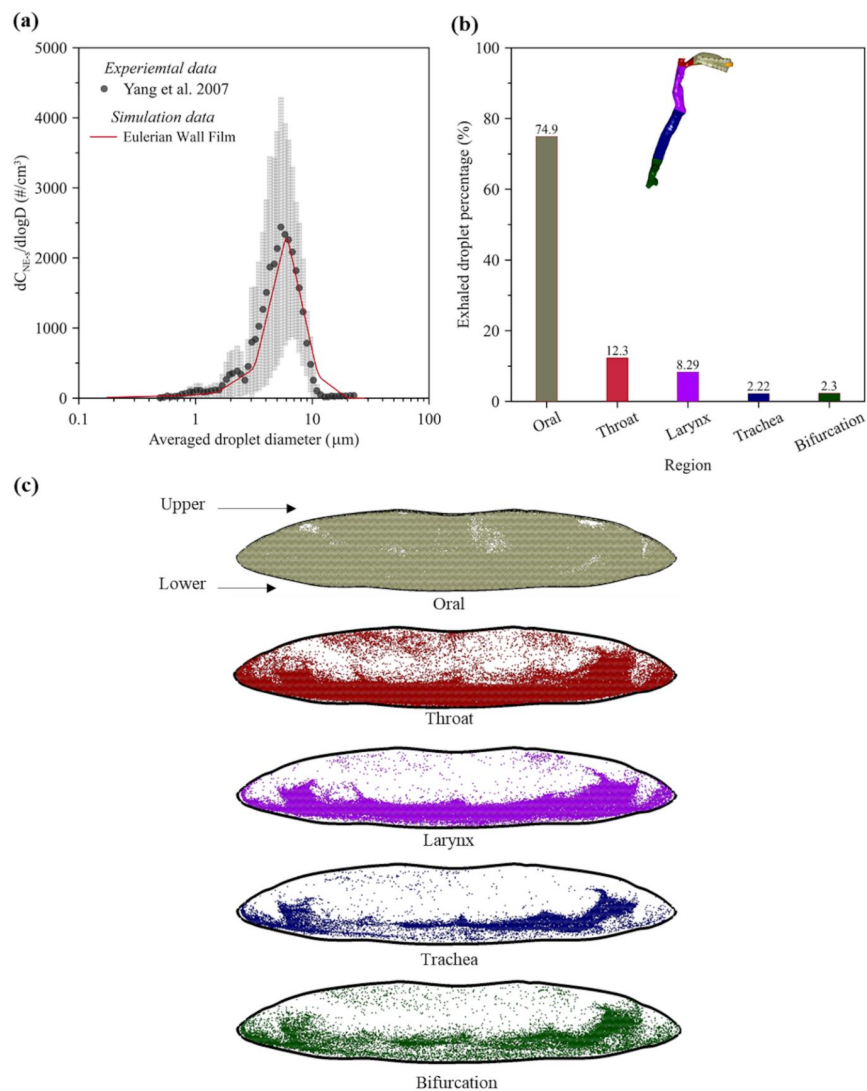
FIG. 6. (a) Validation of total concentration of exhaled droplets after one single cough event. (b) The percentage of exhaled droplets following their site origin. (c) Spatial distribution of exhaled droplets on the mouth opening after a single coughing episode.

576

577

37

(a)

(b)
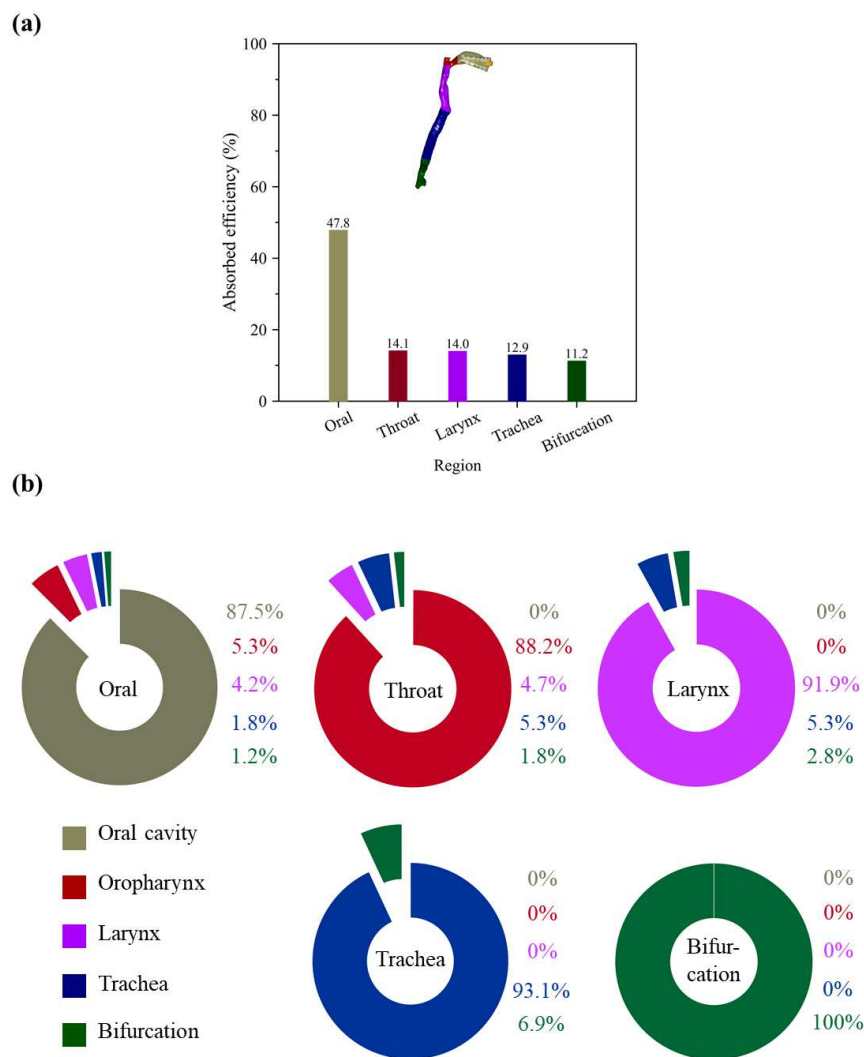
FIG. 7. (a) Total absorbed efficiency of the generated droplets on the inner surface of the airway region. (b) The absorption efficiency rate for different droplet source locations.

578

579
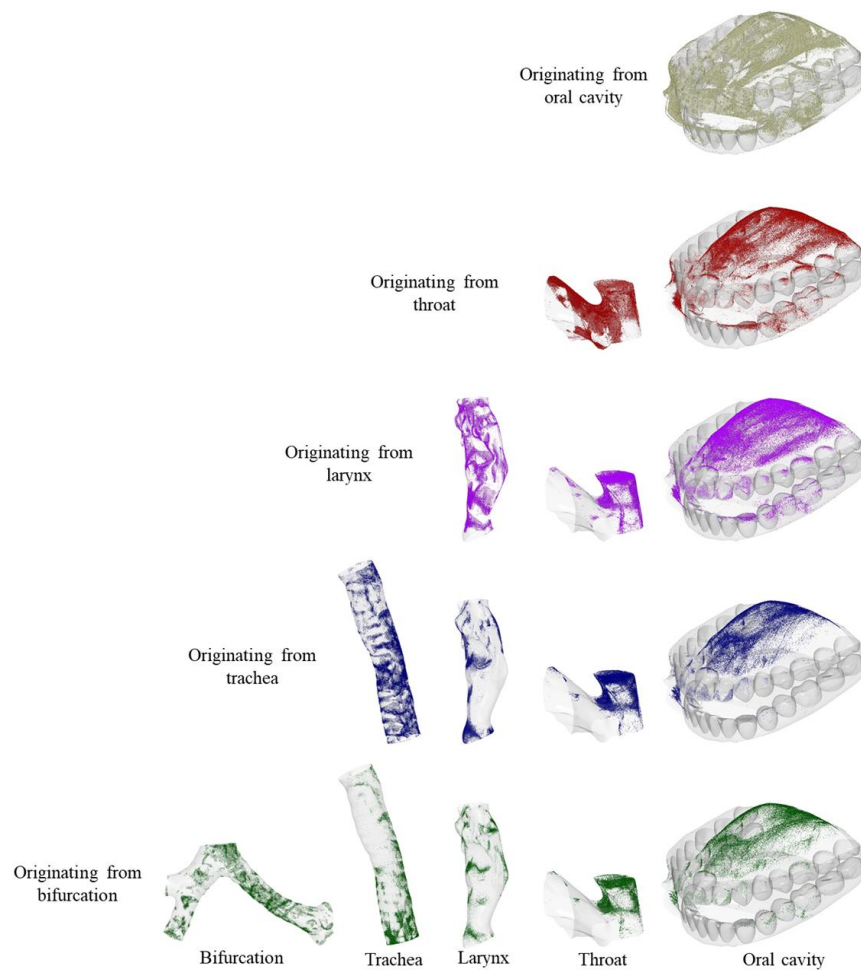
FIG. 8. Visualization of the absorbed droplets in local regions of the oral-tracheal model (column) derived from a specific location (row).

580

581
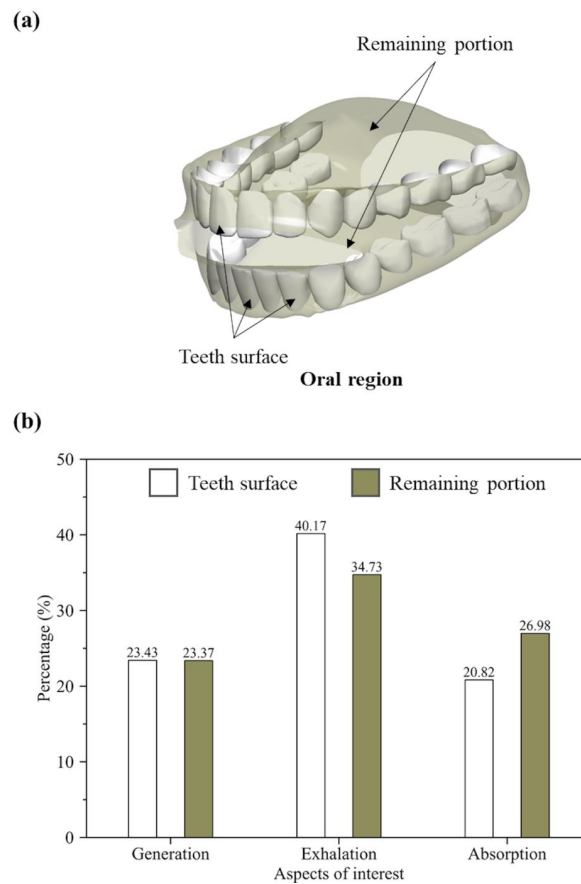
FIG. 9. (a) Outline of the oral cavity, including teeth surface and the remaining regions. (b)The total percentage of generation, exhalation, and absorption of droplets collapsed for the teeth surface and remaining portion.

582

583

584

585

586

(a)

0.04 s   0.077 s

0.0   5.0

[Pa]

Instantaneous
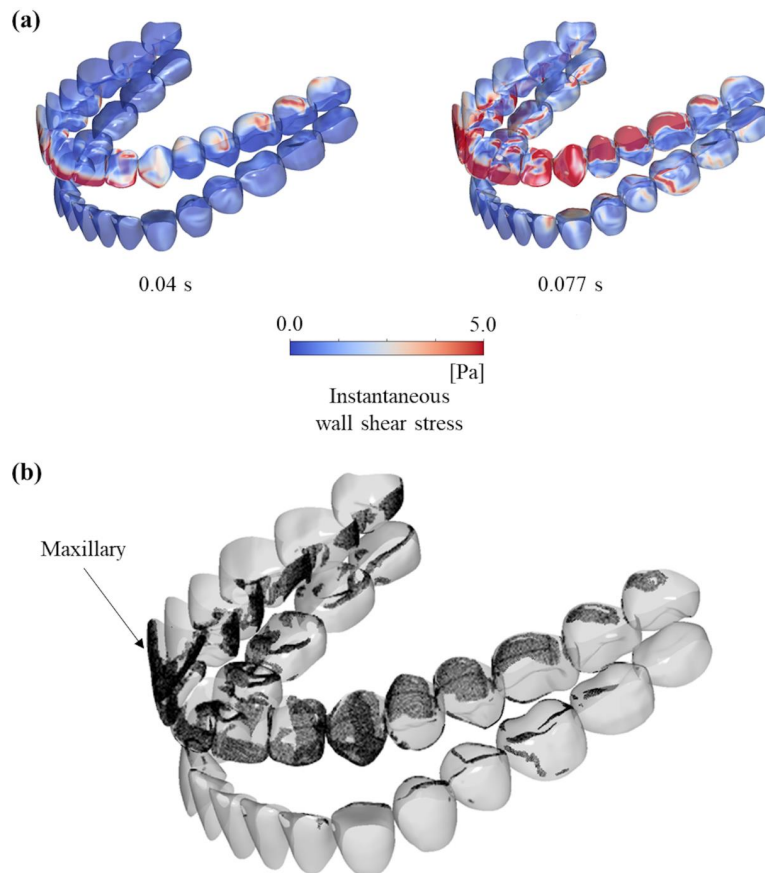wall shear stress

(b)

Maxillary

FIG. 10. (a) The instantaneous wall shear stress distribution on the teeth surface at 0.04 s (left) and 0.077 s (right). (b) Generated location and distribution of droplets on the teeth surface during coughing.
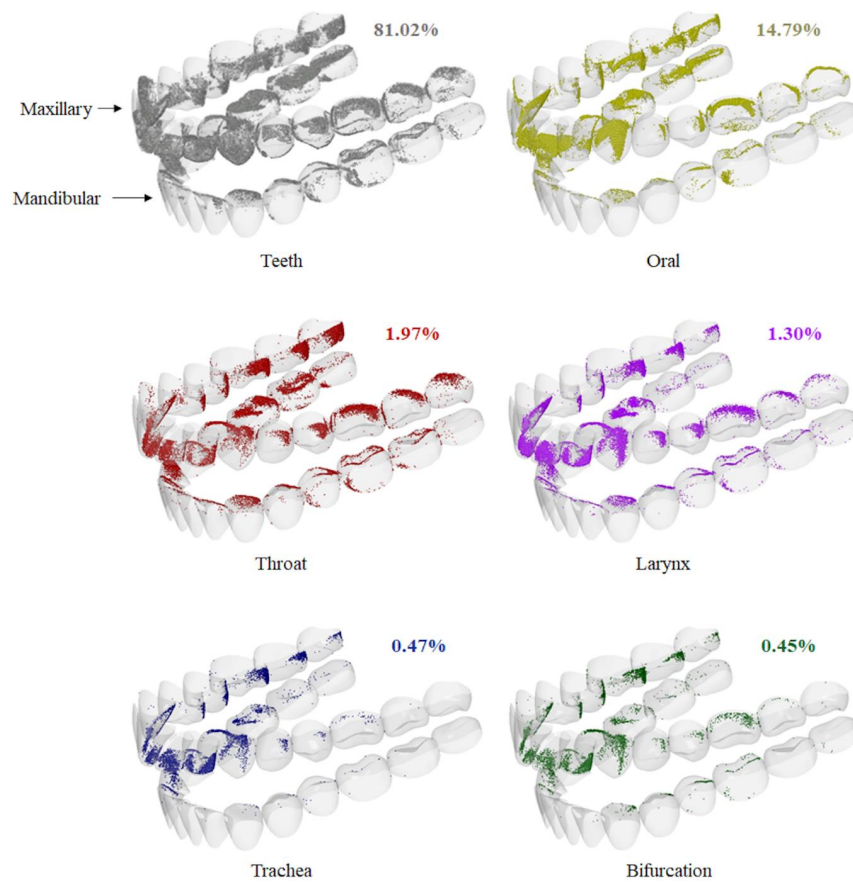
587

588

589

590

591

FIG. 11. 3D visualization of deposited droplets on the teeth surface colored by where the droplet was produced.

592

593

594

595

596

42

597 **VII. TABLES**

598 TABLE I. Numerical boundary conditions for the coughing airflow simulation.

Parameter	Information
Algorithm	SIMPLE (Semi-Implicit Method for Pressured Linked Equations
Convection scheme	Second order upwind
Density (kg/m^3)	1.185
Viscosity (kg/m s)	1.81×10^{-5}
Averaged cough peak flow rate (L/s)	5.75
Averaged cough exhaled volume (cm^3)	1,000
Total simulation time (s)	0.5
Time step size (s)	0.001

599

600 TABLE II. Initial parameter for Eulerian Wall film model.

Parameter	Value
Critical shear stress – CSS (Pa)	5
Diameter coefficient	0.0003
Mass coefficient	0.25
Surface tension (N/m)	0.0589

601
602
603
604
605
606
607
608
609
610

611   TABLE III. Classification of droplet size bin.

Droplet size bin (μm)	Averaged size (μm)
0.1 – 0.25	0.175
0.25 – 0.5	0.375
0.5 – 0.75	0.625
0.75 – 1.0	0.875
1.0 – 2.0	1.5
2.0 – 4.0	3.0
4.0 – 8.0	6.0
8.0 – 16.0	12.0
16.0 – 24.0	20.0
24.0 – 32.0	28.0

612
613
614
615
616
617
618
619
620
621
622
623
624
625
626
627
628
629
630
631
632

44

633 TABLE IV. Generated, exhaled, and absorbed efficiency of droplets during the coughing event
634 following the droplet size bin.

Droplet size bin(μm)	Generated percentage-$\eta_{G\text{-}s}$ [a] (%)	Exhaled percentage-$\eta_{E\text{-}s}$ [b] (%)	Absorbed percentage-$\eta_{A\text{-}s}$ [c] (%)
0.1 – 0.25	0.078	0.49	0.044
0.25 – 0.5	0.133	0.79	0.078
0.5 – 0.75	0.149	0.65	0.108
0.75 – 1.0	0.181	0.50	0.157
1.0 – 2.0	1.94	2.60	1.94
2.0 – 4.0	11.81	12.82	11.58
4.0 – 8.0	78.01	73.06	78.47
8.0 – 16.0	7.53	8.93	7.47
16.0 – 24.0	0.15	0.15	0.15
24.0 – 32.0	0.019	0.01	0.003
Total percentage	100	100	100
Total number count	11,594,566 (N_G)	938,206 (N_E)	10,128,559 (N_A)

635 $*$[a,b,c] The percentage was calculated using Equations 15, 16 and 17
636
637
638
639
640
641
642
643
644
645
646
647

648 **VIII.   SUPPLEMENTARY MATERIAL**

649   The supplementary material contains details and discussions regarding the optimization

650 processes for the total mesh counts and the initial parameters for the EWF model, such as

651 critical shear stress – *CSS* and diameter coefficient – *F*. In addition, detailed boundary

652 conditions and results, which serve to reinforce the reliability of employing the EWF model to

653 simulate the interaction between the free-stream flow and the lining fluid on the surface, are

654 provided.

655 **IX. LIMITATIONS**

656   This study focused on a specific oral-tracheal model, which did not cover the individual-

657 related variability. Besides, it is notable that the initial parameters for the EWF model including

658 critical shear stress – *CSS* and diameter coefficient – *F* were emphasized by the individual

659 structure and numerical boundary conditions of this study. In addition, a rigid airway model

660 was assumed, which is the opposite of the elastic nature of the respiratory tract and ignores

661 glottis deformation during coughing.

46

REFERENCES

Alexander-Brett, J., & Holtzman, M. J. (2015). Virus Infection of Airway Epithelial Cells. In *Mucosal Immunology* (pp. 1013–1021). Elsevier. https://doi.org/10.1016/B978-0-12-415847-4.00053-7

Aljabair, S., Alesbe, I., & Alkhalaf, A. (2023). CFD modeling of influenza virus diffusion during coughing and breathing in a ventilated room. *Journal of Thermal Engineering*, 127–137. https://doi.org/10.18186/thermal.1243491

Ansys® Academic Fluent, Release 2022 R2, Theory Guide, Eulerian Wall Films, ANSYS, Inc.

Anzai, H., Shindo, Y., Kohata, Y., Hasegawa, M., Takana, H., Matsunaga, T., Akaike, T., & Ohta, M. (2022). Coupled discrete phase model and Eulerian wall film model for numerical simulation of respiratory droplet generation during coughing. *Scientific Reports*, *12*(1), 14849. https://doi.org/10.1038/s41598-022-18788-3

Archer, J., McCarthy, L. P., Symons, H. E., Watson, N. A., Orton, C. M., Browne, W. J., Harrison, J., Moseley, B., Philip, K. E. J., Calder, J. D., Shah, P. L., Bzdek, B. R., Costello, D., & Reid, J. P. (2022). Comparing aerosol number and mass exhalation rates from children and adults during breathing, speaking and singing. *Interface Focus*, *12*(2), 20210078. https://doi.org/10.1098/rsfs.2021.0078

Assy, Z., Jager, D. H. J., Brand, H. S., & Bikker, F. J. (2022). Salivary film thickness and MUC5B levels at various intra-oral surfaces. *Clinical Oral Investigations*, *27*(2), 859–869. https://doi.org/10.1007/s00784-022-04626-3

Bahramian, A. (2023). Influence of indoor environmental conditions on airborne transmission and lifetime of sneeze droplets in a confined space: A way to reduce COVID-19 spread. *Environmental Science and Pollution Research*, *30*(15), 44067–44085. https://doi.org/10.1007/s11356-023-25421-x

Bahramian, A., & Ahmadi, G. (2023). Effect of sneeze flow velocity profiles on the respiratory droplets dispersion in a confined space: An experimental and computational fluid dynamics study. *Physics of Fluids*, *35*(6), 063330. https://doi.org/10.1063/5.0151254

Bourouiba, L. (2021). The Fluid Dynamics of Disease Transmission. *Annual Review of Fluid Mechanics*, *53*(1), 473–508. https://doi.org/10.1146/annurev-fluid-060220-113712

Bourouiba, L., Dehandschoewercker, E., & Bush, J. W. M. (2014). Violent expiratory events: On coughing and sneezing. *Journal of Fluid Mechanics*, *745*, 537–563. https://doi.org/10.1017/jfm.2014.88

Calmet, H., Inthavong, K., Both, A., Surapaneni, A., Mira, D., Egukitza, B., & Houzeaux, G. (2021). Large eddy simulation of cough jet dynamics, droplet transport, and inhalability over a ten minute exposure. *Physics of Fluids*, *33*(12), 125122. https://doi.org/10.1063/5.0072148

Chao, C. Y. H., Wan, M. P., Morawska, L., Johnson, G. R., Ristovski, Z. D., Hargreaves, M.,

704   Mengersen, K., Corbett, S., Li, Y., Xie, X., & Katoshevski, D. (2009). Characterization
705   of expiration air jets and droplet size distributions immediately at the mouth opening.
706   *Journal of Aerosol Science*, *40*(2), 122–133.
707   https://doi.org/10.1016/j.jaerosci.2008.10.003

708   Churchyard, G., Kim, P., Shah, N. S., Rustomjee, R., Gandhi, N., Mathema, B., Dowdy, D.,
709   Kasmar, A., & Cardenas, V. (2017). What We Know About Tuberculosis Transmission:
710   An Overview. *The Journal of Infectious Diseases*, *216*(suppl_6), S629–S635.
711   https://doi.org/10.1093/infdis/jix362

712   Collins, L. M. C., & Dawes, C. (1987). The Surface Area of the Adult Human Mouth and
713   Thickness of the Salivary Film Covering the Teeth and Oral Mucosa. *Journal of Dental
714   Research*, *66*(8), 1300–1302. https://doi.org/10.1177/00220345870660080201

715   Dbouk, T., & Drikakis, D. (2020). On coughing and airborne droplet transmission to humans.
716   *Physics of Fluids*, *32*(5), 053310. https://doi.org/10.1063/5.0011960

717   Dhand, R., & Li, J. (2020). Coughs and Sneezes: Their Role in Transmission of Respiratory
718   Viral Infections, Including SARS-CoV-2. *American Journal of Respiratory and Critical
719   Care Medicine*, *202*(5), 651–659. https://doi.org/10.1164/rccm.202004-1263PP

720   Elcner, J., Lizal, F., Jedelsky, J., Jicha, M., & Chovancova, M. (2016). Numerical investigation
721   of inspiratory airflow in a realistic model of the human tracheobronchial airways and a
722   comparison with experimental results. *Biomechanics and Modeling in Mechanobiology*,
723   *15*(2), 447–469. https://doi.org/10.1007/s10237-015-0701-1

724   Gralton, J., Tovey, E. R., McLaws, M.-L., & Rawlinson, W. D. (2013). Respiratory virus RNA
725   is detectable in airborne and droplet particles: Viral RNA in Airborne and Droplet
726   Particles. *Journal of Medical Virology*, *85*(12), 2151–2159.
727   https://doi.org/10.1002/jmv.23698

728   Guo, Y., Wei, J., Ou, C., Liu, L., Sadrizadeh, S., Jin, T., Tang, L., Zhang, Y., & Li, Y. (2020).
729   Deposition of droplets from the trachea or bronchus in the respiratory tract during
730   exhalation: A steady-state numerical investigation. *Aerosol Science and Technology*,
731   *54*(8), 869–879. https://doi.org/10.1080/02786826.2020.1772459

732   Gupta, J. K., Lin, C.-H., & Chen, Q. (2009). Flow dynamics and characterization of a cough:
733   Flow dynamics and characterization of a cough. *Indoor Air*, *19*(6), 517–525.
734   https://doi.org/10.1111/j.1600-0668.2009.00619.x

735   Han, M., Ooka, R., Kikumoto, H., Oh, W., Bu, Y., & Hu, S. (2021). Measurements of exhaled
736   airflow velocity through human coughs using particle image velocimetry. *Building and
737   Environment*, *202*, 108020. https://doi.org/10.1016/j.buildenv.2021.108020

738   Harrison, J., Saccente-Kennedy, B., Orton, C. M., McCarthy, L. P., Archer, J., Symons, H. E.,
739   Szczepanska, A., Watson, N. A., Browne, W. J., Moseley, B., Philip, K. E. J., Hull, J.
740   H., Calder, J. D., Costello, D., Shah, P. L., Epstein, R., Reid, J. P., & Bzdek, B. R. (2023).
741   Emission rates, size distributions, and generation mechanism of oral respiratory

742 droplets. *Aerosol   Science   and   Technology*,   1–13.
743   https://doi.org/10.1080/02786826.2022.2158778

744 Hegland, K. W., Troche, M. S., & Davenport, P. W. (2013). Cough expired volume and airflow
745   rates   during   sequential   induced   cough. *Frontiers   in   Physiology*,   *4*.
746   https://doi.org/10.3389/fphys.2013.00167

747 Hossain, M., Chinenye-Kanu, N., Faisal, N. H., Prathuru, A., Asim, T., & Banik, S. (2023).
748   Numerical Prediction of the Effect of Thermal Plume of a Standing Human on the
749   Airborne Aerosol Flow in a Room: Assessment of the Social Distancing Rule. *Aerosol
750   Science and Engineering*, *7*(1), 96–106. https://doi.org/10.1007/s41810-022-00165-2

751 Huang, N., Pérez, P., Kato, T., Mikami, Y., Okuda, K., Gilmore, R. C., Conde, C. D., Gasmi,
752   B., Stein, S., Beach, M., Pelayo, E., Maldonado, J. O., Lafont, B. A., Jang, S.-I., Nasir,
753   N., Padilla, R. J., Murrah, V. A., Maile, R., Lovell, W., … Byrd, K. M. (2021). SARS-
754   CoV-2 infection of the oral cavity and saliva. *Nature Medicine*, *27*(5), 892–903.
755   https://doi.org/10.1038/s41591-021-01296-8

756 Inthavong, K. (2020). From indoor exposure to inhaled particle deposition: A multiphase
757   journey of inhaled particles. *Experimental and Computational Multiphase Flow*, *2*(2),
758   59–78. https://doi.org/10.1007/s42757-019-0046-6

759 Ito, K. (2016). Toward the development of an *in silico* human model for indoor environmental
760   design. *Proceedings   of   the   Japan   Academy,   Series   B*, *92*(7),   185–203.
761   https://doi.org/10.2183/pjab.92.185

762 Jayaweera, M., Perera, H., Gunawardana, B., & Manatunge, J. (2020). Transmission of
763   COVID-19 virus by droplets and aerosols: A critical review on the unresolved
764   dichotomy.   *Environmental   Research*,   *188*,   109819.
765   https://doi.org/10.1016/j.envres.2020.109819

766 Johnson, G. R., Morawska, L., Ristovski, Z. D., Hargreaves, M., Mengersen, K., Chao, C. Y.
767   H., Wan, M. P., Li, Y., Xie, X., Katoshevski, D., & Corbett, S. (2011). Modality of
768   human expired aerosol size distributions. *Journal of Aerosol Science*, *42*(12), 839–851.
769   https://doi.org/10.1016/j.jaerosci.2011.07.009

770 Jones, R. M., & Brosseau, L. M. (2015). Aerosol Transmission of Infectious Disease. *Journal
771   of   Occupational   &   Environmental   Medicine*,   *57*(5),   501–508.
772   https://doi.org/10.1097/JOM.0000000000000448

773 Kakimpa, B., Morvan, H. P., & Hibberd, S. (2015). Solution Strategies for Thin Film Rimming
774   Flow   Modelling. *Volume   5C: Heat   Transfer*,   V05CT15A026.
775   https://doi.org/10.1115/GT2015-43503

776 Khoa, N. D., Li, S., Phuong, N. L., Kuga, K., Yabuuchi, H., Kan-O, K., Matsumoto, K., & Ito,
777   K. (2023). Computational fluid-particle dynamics modeling of ultrafine to coarse
778   particles deposition in the human respiratory system, down to the terminal bronchiole.
779   *Computer   Methods   and   Programs   in   Biomedicine*,   *237*,   107589.

780   https://doi.org/10.1016/j.cmpb.2023.107589

781   Khoa, N. D., Phuong, N. L., Tani, K., Inthavong, K., & Ito, K. (2023). In-silico decongested

782   trial effects on the impaired breathing function of a bulldog suffering from severe

783   brachycephalic obstructive airway syndrome. *Computer Methods and Programs in*

784   *Biomedicine*, *228*, 107243. https://doi.org/10.1016/j.cmpb.2022.107243

785   Kou, G., Li, X., Wang, Y., Lin, M., Zeng, Y., Yang, X., Yang, Y., & Gan, Z. (2018). CFD

786   Simulation of Airflow Dynamics During Cough Based on CT-Scanned Respiratory

787   Airway Geometries. *Symmetry*, *10*(11), 595. https://doi.org/10.3390/sym10110595

788   Kuga, K., Ito, K., Chen, W., Wang, P., Fowles, J., & Kumagai, K. (2021). Secondary indoor air

789   pollution and passive smoking associated with cannabis smoking using electric

790   cigarette device–demonstrative in silico study. *PLOS Computational Biology*, *17*(5),

791   e1009004. https://doi.org/10.1371/journal.pcbi.1009004

792   Kuga, K., Kizuka, R., Khoa, N. D., & Ito, K. (2023). Effect of transient breathing cycle on the

793   depositionÂ of micro and nanoparticles on respiratory walls. *Computer Methods and*

794   *Programs in Biomedicine*, *236*, 107501. https://doi.org/10.1016/j.cmpb.2023.107501

795   Kuga, K., Sakamoto, M., Wargocki, P., & Ito, K. (2022). Prediction of exhaled carbon dioxide

796   concentration using a computer-simulated person that included alveolar gas exchange.

797   *Indoor Air*, *32*(8).

798   Li, A., & Ahmadi, G. (1992). Dispersion and Deposition of Spherical Particles from Point

799   Sources in a Turbulent Channel Flow. *Aerosol Science and Technology*, *16*(4), 209–226.

800   https://doi.org/10.1080/02786829208959550

801   Li, H., Kuga, K., & Ito, K. (2022). SARS-CoV-2 Dynamics in the Mucus Layer of the Human

802   Upper Respiratory Tract Based on Host–Cell Dynamics. *Sustainability*, *14*(7), 3896.

803   https://doi.org/10.3390/su14073896

804   Li, H., Leong, F. Y., Xu, G., Kang, C. W., Lim, K. H., Tan, B. H., & Loo, C. M. (2021). Airborne

805   dispersion of droplets during coughing: A physical model of viral transmission.

806   *Scientific Reports*, *11*(1), 4617. https://doi.org/10.1038/s41598-021-84245-2

807   Li, X., Mak, C. M., Ai, Z., Ma, K. W., & Wong, H. M. (2023). Numerical investigation of the

808   impacts of environmental conditions and breathing rate on droplet transmission during

809   dental service. *Physics of Fluids*, *35*(4), 043332. https://doi.org/10.1063/5.0144647

810   Lindsley, W. G., Pearce, T. A., Hudnall, J. B., Davis, K. A., Davis, S. M., Fisher, M. A., Khakoo,

811   R., Palmer, J. E., Clark, K. E., Celik, I., Coffey, C. C., Blachere, F. M., & Beezhold, D.

812   H. (2012). Quantity and Size Distribution of Cough-Generated Aerosol Particles

813   Produced by Influenza Patients During and After Illness. *Journal of Occupational and*

814   *Environmental   Hygiene*,   *9*(7),   443–449.

815   https://doi.org/10.1080/15459624.2012.684582

816   Mariam, Magar, A., Joshi, M., Rajagopal, P. S., Khan, A., Rao, M. M., & Sapra, B. K. (2021).

817   CFD Simulation of the Airborne Transmission of COVID-19 Vectors Emitted during

818   Respiratory Mechanisms: Revisiting the Concept of Safe Distance. *ACS Omega*, *6*(26),

819   16876–16889. https://doi.org/10.1021/acsomega.1c01489

820 Morawska, L. (2006). Droplet fate in indoor environments, or can we prevent the spread of

821   infection? *Indoor Air*, *16*(5), 335–347. https://doi.org/10.1111/j.1600-

822   0668.2006.00432.x

823 Morawska, L., Johnson, G. R., Ristovski, Z. D., Hargreaves, M., Mengersen, K., Corbett, S.,

824   Chao, C. Y. H., Li, Y., & Katoshevski, D. (2009). Size distribution and sites of origin of

825   droplets expelled from the human respiratory tract during expiratory activities. *Journal*

826   *of Aerosol Science*, *40*(3), 256–269. https://doi.org/10.1016/j.jaerosci.2008.11.002

827 Murga, A., Bale, R., Li, C.-G., Ito, K., & Tsubokura, M. (2023). Large eddy simulation of

828   droplet transport and deposition in the human respiratory tract to evaluate inhalation

829   risk. *PLOS Computational Biology*, *19*(3), e1010972.

830   https://doi.org/10.1371/journal.pcbi.1010972

831 Nie, Z., Chen, Y., & Deng, M. (2022). Quantitative evaluation of precautions against the

832   COVID-19 indoor transmission through human coughing. *Scientific Reports*, *12*(1),

833   22573. https://doi.org/10.1038/s41598-022-26837-0

834 Nishandar, S. R., He, Y., Princevac, M., & Edwards, R. D. (2023). Fate of Exhaled Droplets

835   From Breathing and Coughing in Supermarket Checkouts and Passenger Cars.

836   *Environmental Health Insights*, *17*, 117863022211482.

837   https://doi.org/10.1177/11786302221148274

838 Pairetti, C., Villiers, R., & Zaleski, S. (2021). On shear layer atomization within closed

839   channels: Numerical simulations of a cough-replicating experiment. *Computers &*

840   *Fluids*, *231*, 105125. https://doi.org/10.1016/j.compfluid.2021.105125

841 Payri, R., Martí-Aldaraví, P., Quintero, P. M., & Marco-Gimeno, J. (2021). LARGE EDDY

842   SIMULATION FOR THE PREDICTION OF HUMAN COUGHING. *Atomization and*

843   *Sprays*, *31*(9), 49–73. https://doi.org/10.1615/AtomizSpr.2021037129

844 Paz, C., Suárez, E., Parga, O., & Vence, J. (2017). Glottis effects on the cough clearance process

845   simulated with a CFD dynamic mesh and Eulerian wall film model. *Computer Methods*

846   *in Biomechanics and Biomedical Engineering*, *20*(12), 1326–1338.

847   https://doi.org/10.1080/10255842.2017.1360872

848 Paz, C., Suárez, E., & Vence, J. (2017). CFD transient simulation of the cough clearance

849   process using an Eulerian wall film model. *Computer Methods in Biomechanics and*

850   *Biomedical Engineering*, *20*(2), 142–152.

851   https://doi.org/10.1080/10255842.2016.1206532

852 Paz, C., Suárez, E., Vence, J., & Cabarcos, A. (2019). Analysis of the volume of fluid (VOF)

853   method for the simulation of the mucus clearance process with CFD. *Computer*

854   *Methods in Biomechanics and Biomedical Engineering*, *22*(5), 547–566.

855   https://doi.org/10.1080/10255842.2019.1569637

856 Phuong, N. L., & Ito, K. (2015). Investigation of flow pattern in upper human airway including
857   oral and nasal inhalation by PIV and CFD. *Building and Environment*, *94*, 504–515.
858   https://doi.org/10.1016/j.buildenv.2015.10.002
859 Piret, J., & Boivin, G. (2021). Pandemics Throughout History. *Frontiers in Microbiology*, *11*,
860   631736. https://doi.org/10.3389/fmicb.2020.631736
861 Pöhlker, M. L., Krüger, O. O., Förster, J.-D., Berkemeier, T., Elbert, W., Fröhlich-Nowoisky,
862   J., Pöschl, U., Pöhlker, C., Bagheri, G., Bodenschatz, E., Huffman, J. A., Scheithauer,
863   S., & Mikhailov, E. (2021). *Respiratory aerosols and droplets in the transmission of*
864   *infectious diseases* (arXiv:2103.01188). arXiv. http://arxiv.org/abs/2103.01188
865 Rajendran, R. R., & Banerjee, A. (2019). Mucus transport and distribution by steady expiration
866   in an idealized airway geometry. *Medical Engineering & Physics*, *66*, 26–39.
867   https://doi.org/10.1016/j.medengphy.2019.02.006
868 Ren, S., Cai, M., Shi, Y., Luo, Z., & Wang, T. (2022). Influence of cough airflow characteristics
869   on respiratory mucus clearance. *Physics of Fluids*, *34*(4), 041911.
870   https://doi.org/10.1063/5.0088100
871 Ren, S., Li, W., Wang, L., Shi, Y., Cai, M., Hao, L., Luo, Z., Niu, J., Xu, W., & Luo, Z. (2020).
872   Numerical Analysis of Airway Mucus Clearance Effectiveness Using Assisted
873   Coughing Techniques. *Scientific Reports*, *10*. https://doi.org/10.1038/s41598-020-
874   58922-7
875 Ren, S., Shi, Y., Cai, M., Zhao, H., & Zhang, Z. (2018). ANSYS-MATLAB co-simulation of
876   mucus flow distribution and clearance effectiveness of a new simulated cough device.
877   *International Journal for Numerical Methods in Biomedical Engineering*, *34*(6).
878   https://doi.org/10.1002/cnm.2978
879 Saffman, P. G. (1965). The lift on a small sphere in a slow shear flow. *Journal of Fluid*
880   *Mechanics*, *22*(2), 385–400. https://doi.org/10.1017/S0022112065000824
881 Schaefer, A., & Lai, S. K. (2022). The biophysical principles underpinning muco-trapping
882   functions of antibodies. *Human Vaccines & Immunotherapeutics*, *18*(2), 1939605.
883   https://doi.org/10.1080/21645515.2021.1939605
884 Seminara, G., Carli, B., Forni, G., Fuzzi, S., Mazzino, A., & Rinaldo, A. (2020). Biological
885   fluid dynamics of airborne COVID-19 infection. *Rendiconti Lincei. Scienze Fisiche e*
886   *Naturali*, *31*(3), 505–537. https://doi.org/10.1007/s12210-020-00938-2
887 SeyedAlinaghi, S., Karimi, A., Mojdeganlou, H., Pashaei, Z., Mirzapour, P., Shamsabadi, A.,
888   Barzegary, A., Afroughi, F., Dehghani, S., Janfaza, N., Fakhfouri, A., Khodaei, S.,
889   Mehraen, E., & Dadras, O. (2022). Minimum infective dose of severe acute respiratory
890   syndrome coronavirus 2 based on the current evidence: A systematic review. *SAGE*
891   *Open Medicine*, *10*, 205031212211150. https://doi.org/10.1177/20503121221115053
892 Shelley, D. A., Sih, B. L., & Ng, L. J. (2014). *An integrated physiology model to study regional*
893   *lung damage effects and the physiologic response*. 19.

894 Sosnowski, T. R. (2021). Inhaled aerosols: Their role in COVID-19 transmission, including
895 biophysical interactions in the lungs. *Current Opinion in Colloid & Interface Science*,
896 *54*, 101451. https://doi.org/10.1016/j.cocis.2021.101451

897 Stadnytskyi, V., Anfinrud, P., & Bax, A. (2021). Breathing, speaking, coughing or sneezing:
898 What drives transmission of SARS-CoV-2? *Journal of Internal Medicine*, *290*(5),
899 1010–1027. https://doi.org/10.1111/joim.13326

900 To, K. K.-W., Tsang, O. T.-Y., Yip, C. C.-Y., Chan, K.-H., Wu, T.-C., Chan, J. M.-C., Leung,
901 W.-S., Chik, T. S.-H., Choi, C. Y.-C., Kandamby, D. H., Lung, D. C., Tam, A. R., Poon,
902 R. W.-S., Fung, A. Y.-F., Hung, I. F.-N., Cheng, V. C.-C., Chan, J. F.-W., & Yuen, K.-Y.
903 (2020). Consistent Detection of 2019 Novel Coronavirus in Saliva. *Clinical Infectious
904 Diseases*, *71*(15), 841–843. https://doi.org/10.1093/cid/ciaa149

905 Wang, C. C., Prather, K. A., Sznitman, J., Jimenez, J. L., Lakdawala, S. S., Tufekci, Z., & Marr,
906 L. C. (2021). Airborne transmission of respiratory viruses. *Science*, *373*(6558),
907 eabd9149. https://doi.org/10.1126/science.abd9149

908 Wang, C., Yoo, S.-J., Tanabe, S., & Ito, K. (2020). Investigation of transient and heterogeneous
909 micro-climate around a human body in an enclosed personalized work environment.
910 *Energy and Built Environment*, *1*(4), 423–431.
911 https://doi.org/10.1016/j.enbenv.2020.04.011

912 Wang, H., Li, Z., Zhang, X., Zhu, L., Liu, Y., & Wang, S. (2020). The motion of respiratory
913 droplets produced by coughing. *Physics of Fluids*, *32*(12), 125102.
914 https://doi.org/10.1063/5.0033849

915 Wei, J., & Li, Y. (2016). Airborne spread of infectious agents in the indoor environment.
916 *American Journal of Infection Control*, *44*(9), S102–S108.
917 https://doi.org/10.1016/j.ajic.2016.06.003

918 Widders, A., Broom, A., & Broom, J. (2020). SARS-CoV-2: The viral shedding vs infectivity
919 dilemma. *Infection, Disease & Health*, *25*(3), 210–215.
920 https://doi.org/10.1016/j.idh.2020.05.002

921 Wölfel, R., Corman, V. M., Guggemos, W., Seilmaier, M., Zange, S., Müller, M. A., Niemeyer,
922 D., Jones, T. C., Vollmar, P., Rothe, C., Hoelscher, M., Bleicker, T., Brünink, S.,
923 Schneider, J., Ehmann, R., Zwirglmaier, K., Drosten, C., & Wendtner, C. (2020).
924 Virological assessment of hospitalized patients with COVID-2019. *Nature*, *581*(7809),
925 465–469. https://doi.org/10.1038/s41586-020-2196-x

926 Wyllie, A. L., Fournier, J., Casanovas-Massana, A., Campbell, M., Tokuyama, M., Vijayakumar,
927 P., Warren, J. L., Geng, B., Muenker, M. C., Moore, A. J., Vogels, C. B. F., Petrone, M.
928 E., Ott, I. M., Lu, P., Venkataraman, A., Lu-Culligan, A., Klein, J., Earnest, R., Simonov,
929 M., … Ko, A. I. (2020). Saliva or Nasopharyngeal Swab Specimens for Detection of
930 SARS-CoV-2. *New England Journal of Medicine*, *383*(13), 1283–1286.
931 https://doi.org/10.1056/NEJMc2016359

932 Yan, J., Grantham, M., Pantelic, J., Bueno De Mesquita, P. J., Albert, B., Liu, F., Ehrman, S.,
933   Milton, D. K., EMIT Consortium, Adamson, W., Beato-Arribas, B., Bischoff, W., Booth,
934   W., Cauchemez, S., Ehrman, S., Enstone, J., Ferguson, N., Forni, J., Gilbert, A., …
935   Tellier, R. (2018). Infectious virus in exhaled breath of symptomatic seasonal influenza
936   cases from a college community. *Proceedings of the National Academy of Sciences*,
937   *115*(5), 1081–1086. https://doi.org/10.1073/pnas.1716561115
938 Yang, S., Lee, G. W. M., Chen, C.-M., Wu, C.-C., & Yu, K.-P. (2007). The Size and
939   Concentration of Droplets Generated by Coughing in Human Subjects. *Journal of
940   Aerosol Medicine*, *20*(4), 484–494. https://doi.org/10.1089/jam.2007.0610
941 Yi, H., Wang, Q., & Feng, Y. (2021). Computational analysis of obstructive disease and cough
942   intensity effects on the mucus transport and clearance in an idealized upper airway
943   model using the volume of fluid method. *Physics of Fluids*, *33*(2), 021903.
944   https://doi.org/10.1063/5.0037764
945 Yoo, S., & Ito, K. (2022). Validation, verification, and quality control of computational fluid
946   dynamics analysis for indoor environments using a computer-simulated person with
947   respiratory tract. *JAPAN ARCHITECTURAL REVIEW*, *5*(4), 714–727.
948   https://doi.org/10.1002/2475-8876.12301
949 Zayas, G., Chiang, M. C., Wong, E., MacDonald, F., Lange, C. F., Senthilselvan, A., & King,
950   M. (2012). Cough aerosol in healthy participants: Fundamental knowledge to optimize
951   droplet-spread infectious respiratory disease management. *BMC Pulmonary Medicine*,
952   *12*(1), 11. https://doi.org/10.1186/1471-2466-12-11
953 Zhou, M., & Zou, J. (2021). A dynamical overview of droplets in the transmission of respiratory
954   infectious diseases. *Physics of Fluids*, *33*(3), 031301.
955   https://doi.org/10.1063/5.0039487
956 Zore, K., Parkhi, G., Sasanapuri, B., & Varghese, A. (2019). 21th Annual CFD Symposium,
957   August 8-9, 2019, Bangalore. *Annual CFD Symposium*, 0–11.
958 Zuo, Y. Y., Uspal, W. E., & Wei, T. (2020). Airborne Transmission of COVID-19: Aerosol
959   Dispersion, Lung Deposition, and Virus-Receptor Interactions. *ACS Nano*, *14*(12),
960   16502–16524. https://doi.org/10.1021/acsnano.0c08484
961

962 **CONFLICT OF INTEREST STATEMENT**

963   The authors declare that they have no competing financial interests or personal

964 relationships that could have influenced the work reported in this paper.

965 **DATA AVAILABILITY**

966   The data supporting this study's findings are available from the corresponding author upon

967   reasonable request.